Received: 19 October 2017 | Revised: 1 April 2018 | Accepted: 3 April 2018

DOI: 10.1002/cne.24480

WILEY JCN RESEARCH IN SYSTEMS NEUROSCIENCE THE JOURNAL OF COMPARATIVE NEUROLOGY

RESEARCH ARTICLE

A 3D MRI-based atlas of a lizard brain

Daniel Hoops[1] | Ester Desfilis[2] | Jeremy F. P. Ullmann[3] | Andrew L. Janke[3] | Timothy Stait-Gardner[4] | Gabriel A. Devenyi[5,6] | William S. Price[4] | Loreta Medina[2] | Martin J. Whiting[7] | J. Scott Keogh[1]

[1]Division of Ecology & Evolution, Research School of Biology, The Australian National University, Canberra, ACT, Australia

[2]Laboratory of Evolutionary and Developmental Neurobiology, Department of Experimental Medicine, Lleida Institute for Biomedical Research Fundació Dr. Pifarré (IRBLleida), University of Lleida, Lleida, Spain

[3]Center for Advanced Imaging, The University of Queensland, Brisbane, QLD, Australia

[4]Nanoscale Organization and Dynamics Group, Western Sydney University, Penrith, NSW, Australia

[5]Douglas Hospital Research Centre, Douglas Mental Health University Institute, Montreal, Quebec, Canada

[6]Department of Psychiatry, McGill University, Montreal, Quebec, Canada

[7]Department of Biological Sciences, Macquarie University, Sydney, NSW, Australia

Correspondence
Email: daniel.hoops@mail.mcgill.ca

Funding information
Government of Australia, Grant/Award Numbers: APA#31/2011, IPRS#1182/2010; National Science and Engineering Research Council of Canada, Grant/Award Number: PGSD3-415253-2012; Quebec Nature and Technology Research Fund, Grant/Award Number: 208332; National Imaging Facility of Australia; Spanish Ministerio de Economía y Competitividad and Fondo Europeo de Desarrollo Regional, Grant/Award Number: BFU2015-68537-R

Abstract

Magnetic resonance imaging (MRI) is an established technique for neuroanatomical analysis, being particularly useful in the medical sciences. However, the application of MRI to evolutionary neuroscience is still in its infancy. Few magnetic resonance brain atlases exist outside the standard model organisms in neuroscience and no magnetic resonance atlas has been produced for any reptile brain. A detailed understanding of reptilian brain anatomy is necessary to elucidate the evolutionary origin of enigmatic brain structures such as the cerebral cortex. Here, we present a magnetic resonance atlas for the brain of a representative squamate reptile, the Australian tawny dragon (Agamidae: *Ctenophorus decresii*), which has been the subject of numerous ecological and behavioral studies. We used a high-field 11.74T magnet, a paramagnetic contrasting-enhancing agent and minimum-deformation modeling of the brains of thirteen adult male individuals. From this, we created a high-resolution three-dimensional model of a lizard brain. The 3D-MRI model can be freely downloaded and allows a better comprehension of brain areas, nuclei, and fiber tracts, facilitating comparison with other species and setting the basis for future comparative evolution imaging studies. The MRI model and atlas of a tawny dragon brain (*Ctenophorus decresii)* can be viewed online and downloaded using the Wiley Biolucida Server at wiley.biolucida.net.

KEYWORDS

brain organization, columnar, evolution, magnetic resonance imaging, neuromeric, prosomeric, reptile

1 | INTRODUCTION

Squamate reptiles (lizards and snakes) comprise the second largest group of terrestrial vertebrates, with more than 10,000 species (Pyron, Burbrink, & Wiens, 2013; Reeder et al., 2015; Uetz & Hošek, 2017). Due to the extent to which they occupy diverse ecological niches, squamates have been recognized as an ideal group for comparative studies of brain evolution and the evolution of brain-behavior relationships (Hoops, 2018). For example, they are an optimal group with which to study comparative cognition (Clark, Amiel, Shine, Noble, & Whiting, 2013; Leal & Powell, 2012; Northcutt, 2013) and its relationship with the evolution of sociality (Whiting & While, 2017). Furthermore, interest in the neurobiology of squamates is increasing, including both single-species studies (Amiel, Bao, & Shine, 2017; Day, Crews, & Wilczynski, 1999; LaDage et al., 2013; LaDage, Riggs, Sinervo, & Pravosudov, 2009; Lutterschmidt & Maine, 2014)

Daniel Hoops and Ester Desfilis contributed equally to this work.

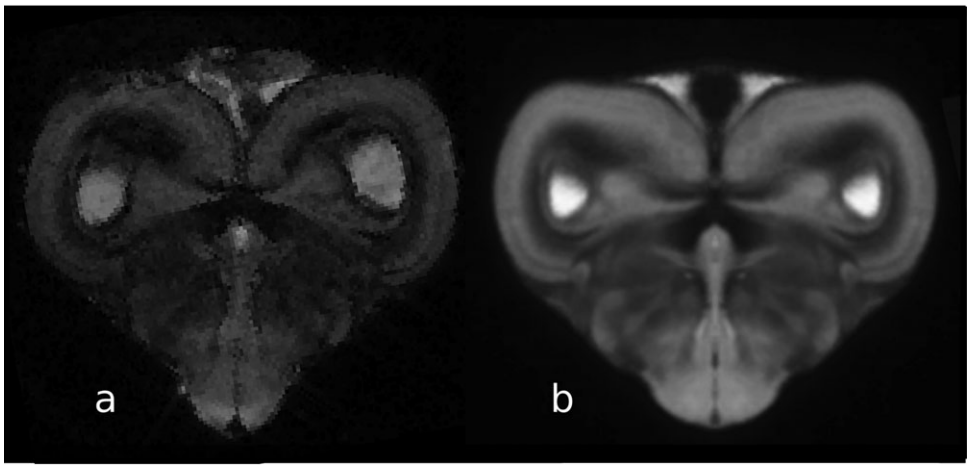

FIGURE 1 A comparison between a coronal section from (a) an MRI image of a single brain and (b) the MRI model of thirteen brains demonstrates that the model has far superior resolution (voxel = 20 μm^3) compared to the image of a single brain (voxel = 50 μm^3)

and comparative studies (Hoops, Ullmann, et al., 2017a; Hoops, Vidal-García, et al., 2017b; Powell & Leal, 2014; Robinson, Patton, Andre, & Johnson, 2015).

Comparative studies on brain anatomy and evolution would be greatly facilitated if the animal's nervous system could be rapidly visualized in an intact head, and even in live specimens (Corfield, Wild, Cowan, Parsons, & Kubke, 2008). Magnetic resonance imaging (MRI) is a noninvasive technique that allows for such visualization. This technique is particularly useful in the case of endangered or protected species, and when working with precious museum specimens that would be destroyed in the process of extracting the brain. From a practical perspective, MRI is advantageous because it does not require any of the labor-intensive tissue processing necessary for histology. The resulting image can be viewed in any plane, allowing for brain regions and fiber tracts to be viewed from multiple orientations throughout their rostral-caudal extent. In addition, MRI can facilitate both inter- and intraspecific comparisons as measurements can be semi-computer-automated (e.g., Lerch et al., 2008).

In order for MRI to facilitate comparative neuroscience, however, MRI atlases must be available for a diversity of animal species. Such atlases are available for brains from most major vertebrate lineages, including bony fishes (Kabli, Alia, Spaink, Verbeek, & De Groot, 2006; Ullmann, Cowin, & Collin, 2010a; Ullmann, Cowin, Kurniawan, & Collin, 2010b), cartilaginous fishes (Yopak & Frank, 2009), birds (Poirier et al., 2008; Vellema, Verschueren, Van Meir, & Van der Linden, 2011), and mammals (Dorr, Lerch, Spring, Kabani, & Henkelman, 2008; Ullmann et al., 2012; Ullmann, Watson, Janke, Kurniawan, & Reutens, 2013a; Ullmann et al., 2013b). To our knowledge, only one published study has used MRI to image the brain of a reptile, the garter snake (*Thamnophis sirtalis*; Anderson, Kabalka, Layne, Dyke, & Burghardt, 2000); however the resolution was not sufficient to distinguish most structures. Developing an MRI atlas of a reptilian brain would be the first step in conducting broad-scale comparative analyses both within reptiles and across all the major vertebrate clades.

Here, we present a detailed description of the brain of an agamid lizard, the Australian tawny dragon (*Ctenophorus decresii*, Duméril & Bibron, 1837; Reptilia: Agamidae), using high-resolution MRI. In the

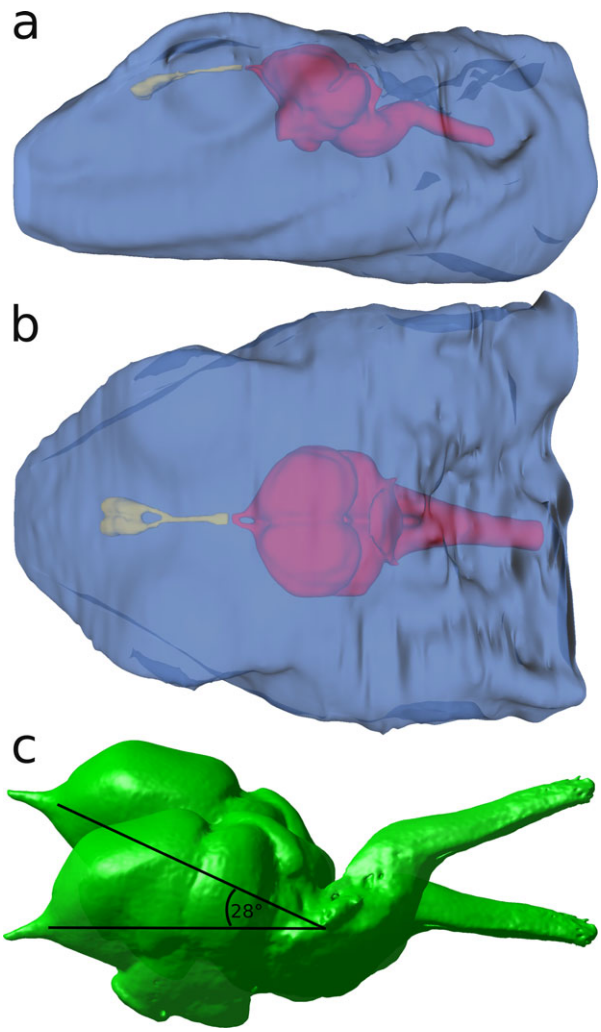

FIGURE 2 A three-dimensional rendering of an MRI of a tawny dragon (*Ctenophorus decresii*) head showing the position of its brain from (a) a lateral perspective and (b) a dorsal perspective. The majority of the brain (in red) is included in this model, however the olfactory tracts and bulbs (in yellow) are excluded. (c) The natural position of the brain inside the tawny dragon head is rotated 28° in the x-plane compared to the position of our model [Color figure can be viewed at wileyonlinelibrary.com]

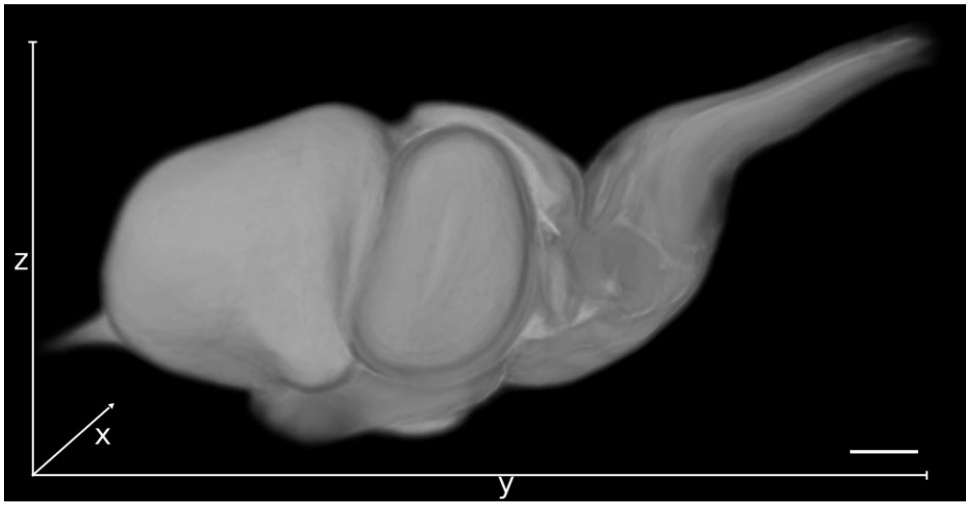

FIGURE 3 Our coordinate system for the lizard brain, demonstrated using a three-dimensional view of the lizard brain model with coordinate axes indicated. The bar in the lower right corner = 1 mm

atlas we identify nuclei, fiber tracts, and other structures throughout the brain in coronal, sagittal, and horizontal orientations. Furthermore, we describe our MRI data with reference to the neuromeric/prosomeric model, in addition to the traditional columnar model, since the former is more natural as it relates to the fundamental divisions of the brain that are shared by all vertebrates (Puelles, 2009; Puelles & Rubenstein, 2015; Puelles, Harrison, Paxinos, & Watson, 2013). This atlas therefore provides a new means of understanding the structure and connectivity of the reptile brain.

2 | METHODS

2.1 | Specimen acquisition

Sixteen male tawny dragons were collected from the southern Flinders Ranges, South Australia. We euthanized each lizard with an injection of 100 mg/kg sodium pentobarbital and an equal volume of 2 mg/mL lignocaine. Each lizard was then intracardially perfused following Hoops (2015). Magnevist was added to the fixative perfusate (4% paraformaldehyde) to maximize image contrast in magnetic resonance imaging (Ullmann, Cowin, & Collin, 2010a). The brains were stored at 4°C in a solution of 0.1% Magnevist and 0.05% sodium azide in phosphate-buffered saline until imaging. The Australian National University's Animal Experimental Ethics Committee approved all research under protocol number A2011-49.

2.2 | Magnetic resonance imaging

Whole-brain images of 13 tawny dragon brains (e.g., Figure 1a) were acquired using a Bruker Avance 11.74 Tesla wide-bore spectrometer (Ettlingen, Germany) with a micro-2.5 imaging probe capable of generating magnetic gradients of 1.50 T/m. Brains were immersed in Fomblin (perfluoropolyether, Grade Y06/6, JAVAC, Sydney, Australia) and placed in a 10 mm diameter Wilmad tube using a custom-built plastic holder (Hyare et al., 2008). Parameters used in the scans were optimized for gray-white matter contrast in the presence of Magnevist. We used a 3D fast gradient-echo sequence (FLASH; T_2*-weighted), with repetition time = 40 ms, echo time = 8 ms, field-of-view = 11 × 11 × 16 mm, and matrix size = 110 × 110 × 160, producing an image with 50 μm^3 isotropic voxels.

For comparison, two brains were embedded in agarose and vibratome-sectioned at 70 μm. Brain sections were stained for 5 min using the DNA-binding stain SYBR-green (Life Technologies Australia, Melbourne, Australia), rinsed in phosphate-buffered saline, mounted in Fluoro-Gel (ProSciTech, Brisbane, Australia), and imaged using Olympus fluorescence light microscopes.

2.3 | Model generation and analysis

To ensure consistent measures of brain morphometry all images were first manually masked such that consistent coverage of brain structures and nerve endings was achieved. In the tawny dragon the olfactory bulbs are small and separated from the brain on long stalks (Figure 2) and we were unable to stabilize their location in the Wilmad tube. Therefore, the olfactory bulbs were included in the masked regions. The manually masked areas were then set to the background value such that they were not included in subsequent calculations.

Thirteen brain image datasets of 50 μm^3 resolution were first reoriented to standard rostro-caudal orientation. All images were then corrected for B0 intensity inhomogeneity using the N3 algorithm (Sled, Zijdenbos, & Evans, 1998). An image with a good signal to noise ratio and no obvious artifacts was then manually selected from the group to create an initial model by blurring. All images were then recursively matched to this evolving model of average structure to create a minimum deformation average with a resulting resolution of 20 μm^3 (Figure 1b). The details of the model creation process can be found in Janke and Ullmann (2015). The fitting stages in this case started at a resolution of 1.28 mm and finished with a resolution of 80 μm^3. The model finished with a resolution of 20 μm^3.

To compare the natural orientation of the tawny dragon brain to the orientation of our model, a representative scan was acquired of a brain within a fully intact tawny dragon head. The brain was automatically segmented from this scan using a combination of registration to

TABLE 1 Legend of abbreviations used in Figures 4–39 in alphabetical order. As per convention, nuclei, areas and other structures are capitalized, while fibre tracks not (Paxinos & Franklin, 2013; Paxinos & Watson, 2013)

Abbreviation	Brain Region	Coronal Figures	Horizontal Figures	Sagittal Figures
*	Blood Vessel	8		
3n	Oculomotor Nerve	14	24, 25	31, 32
3N	Nucleus of the Oculomotor Nerve	14	25, 26	
3ND	Nucleus of the Oculomotor Nerve, dorsal part	15		
3NV	Nucleus of the Oculomotor Nerve, ventral part	15	25	32
3V	Third Ventricle	8, 9, 10, 11, 12, 13	23, 24	
4n	Trochlear Nerve	15, 16	26, 27	31, 32, 33, 34
4N	Nucleus of the Trochlear Nerve	15, 16	26	31, 32
4V	Fourth Ventricle	16, 17, 18, 19, 20	26, 27	
5d	Descending Tract of the Trigeminal Nerve	18, 19, 20		
5DM	Dorsal Motor Nucleus of the Trigeminal Nerve	17		33
5DN	Descending Nucleus of the Trigeminal Nerve	18, 19, 20	25, 26, 27	34
5me	Trigeminal Mesencephalic Tract	16		
5n	Trigeminal Nerve	16	25, 26	33, 34, 35
5Pr	Principal Nucleus of the Trigeminal Nerve	17		34
5Sp	Spinal Nucleus of the Trigeminal Nerve			32
5VM	Ventral Motor Nucleus of the Trigeminal Nerve	17	25	34
6n	Abducens Nerve	17, 18	24, 25	32
6N	Nucleus of the Abducens Nerve	17, 18	26	
7DM	Dorsal Motor Nucleus of the Facial Nerve	18		
7VM	Ventral Motor Nucleus of the Facial Nerve	18		
8n	Statoacoustic Nerve	17, 18	26, 27	32, 33, 34, 35
10DN	Dorsal Motor Nucleus of the Vagus Nerve	19, 20		
10N	Motor Nucleus of the Vagus Nerve	20		
12n	Hypoglossal Nerve	19, 20		
12N	Nucleus of the Hypoglossal Nerve	19, 20		32
a	Alveus	5, 6, 7, 8, 9, 10	27, 28, 29, 30	32, 33, 34, 35
A8	Catecholaminergic Cell Group A8	15	26	
ac	Anterior Commissure	8, 9	26	31, 32
AC	Nucleus of the Anterior Commissure	9		
Acb	Accumbens Nucleus	5, 6, 7	25, 26	31, 32
ADVR	Anterior Dorsal Ventricular Ridge	5, 6, 7, 8	27, 28, 29	32, 33, 34, 35
AHA	Anterior or Alar Hypothalamic Area	10		
AngC	Angular Cochlear Nucleus	17	27	
AO	Anterior Olfactory Nucleus	4	26	32, 33
AOT	Nucleus of the Accessory Olfactory Tract	8		
apc	Anterior Pallial Commissure	8, 9	26, 27	31
Arc	Arcuate Nucleus	11, 12, 13	22	31, 32
AS	Anterior Septal Nucleus	7, 8, 9	28	31
Au	Auricle	16	27	
BAC	Bed Nucleus of the Anterior Commissure	9	25	31
bc	Brachium Conjunctivum	16	26	34
bop	Basal Optic Tract	11, 12, 13, 14	23	
BOp	Nucleus of the Basal Optic Tract	12, 13, 14	25	34
CAq	Cerebral Aqueduct	13, 14, 15		31
CC	Central Canal of the Spinal Cord	21		
Ce	Cerebellum	13, 14, 15, 16, 17	27, 28, 29, 30	31, 32, 33, 34
CeL	Cerebellar Nucleus, lateral part	16	26	
CeM	Cerebellar Nucleus, medial	16		33
CG	Central Grey	12, 13, 14, 15, 16	25, 26, 27	31, 32

TABLE 1 (Continued)

Abbreviation	Brain Region	Coronal Figures	Horizontal Figures	Sagittal Figures
chp	Choroid Plexus	10		32
CPDMCx	Cell Plate of the Dorsomedial Cortex	10		
DB	Nucleus of the Diagonal Band	6, 7	24	32, 33
dc	Dorsal Coclear Tract	17, 18, 19	27	32
DCx	Dorsal Cortex	5, 6, 7, 8, 9, 10	28, 29, 30	33, 34, 35
dcol	Dorsal Column Tract	20, 21		31, 32
DColL	Nucleus of the Dorsal Column, lateral part	19, 20		32
DColM	Nucleus of the Dorsal Column, medial part	19, 20		
DH	Dorsal Horn of the Spinal Cord	21		
DLA	Dorsolateral Amygdala	9	28	35
DLH	Dorsolateral Hypothalamic Nucleus	10, 11	24	32
DLPR	Dorsolateral Pallium, Rostral Part	4		
DLT	Dorsolateral Thalamic Nucleus	10	25, 26	
DLVe	Dorsolateral Vestibular Nucleus	17, 18	27	33, 34
DIRtF	Dorsal Nucleus of the Inferior Reticular Formation	19, 20	25, 26, 27	32, 33
DMCx	Dorsomedial Cortex	5, 6, 7, 8, 9, 10	30	32, 33, 34, 35
DMH	Dorsomedial Hypothalamic Nucleus	11		31
DMS	Dorsal Median Sulcus of the Cerebellum	13, 14, 15, 16		
DMT	Dorsomedial Thalamic Nucleus	10, 11	25, 26	31
DPR	Dorsal Pallium, Rostral Part	4		
DPT	Dorsal Pretectal Nucleus	12	25, 26	33, 34
DS	Dorsal Septal Nucleus	8	27	31
DSC	Dorsal Septal Nucleus, central part	9		
DSD	Dorsal Septal Nucleus, dorsal part	9	27	31
DSt	Dorsal Striatum	5, 6, 7, 8	26	33, 34
DTg	Dorsal Tegmental Nucleus	16		32
Ep	Epiphysis	11, 12	28, 29, 30	31
EPA	Entopeduncular Nucleus, anterior part	10		
EPP	Entopeduncular Nucleus, posterior part	13	24	
EPT	External Pretectal Nucleus	11, 12		34
EW	Edinger-Westphal Nucleus	14		
f	Fornix		25	
fi	Fimbria	10		
fr	Fasciculus Retroflexus	11, 12	25, 26	32
GL	Glomerular Layer of the Cerebellum	15		32
GP	Globus Pallidus	7		
Hb	Habenula	11	27	
hbc	Habenular Commissure	11		31
iarc	Internal Arcuate Fibres	18		
ic	Infima Commissure	19, 20		
IC	Nucleus of the Infima Commissure	20		
ICc	Intercollicular Nucleus	14, 15	27	33, 34
IMLF	Interstitial Nucleus of the Medial Longitudinal Fasciculus	13	25	
iot	Intermediate Olfactory Tract	7		
IPD	Interpeduncular Nucleus, dorsal part	14, 15	24	31
IPV	Interpeduncular Nucleus, ventral part	14, 15	23, 24	31
IR	Inferior Raphe Nucleus	17, 18, 19, 20	24, 25, 26, 27	31
IS	Inferior Septal Nucleus	8, 9		31
IsD	Isthmic Nucleus, Diffuse part	15		34

TABLE 1 (Continued)

Abbreviation	Brain Region	Coronal Figures	Horizontal Figures	Sagittal Figures
IsM	Isthmic Nucleus, Magnocellular part (pre-Isthmic or mesencephalic)	15, 16	26, 27	34
IsP	Isthmic Nucleus, Parvocellular part	16	25, 26	
LA	Lateral Amygdala	9	26, 27	36
LCx	Lateral Cortex	5, 6, 7, 8, 9	28, 29	34, 35, 36
lfb	Lateral Forebrain Bundle	5, 6, 7, 8,	24, 25, 26, 27	32, 33, 34
lfbd	Lateral Forebrain Bundle, dorsal peduncle	10, 11, 12, 13	25	
lfbv	Lateral Forebrain Bundle, ventral peduncle	10, 11, 12, 14	24, 25	34
LGD	Lateral Geniculate Nucleus, dorsal part	10	26	
LGV	Lateral Geniculate Nucleus, ventral part	10, 11	24, 25	33, 34
LHA	Lateral Hypothalamic Area	11, 12, 13	23	32, 33
LHb	Lateral Habenula	10		
LJC	Lateral Juxtacommissural Nucleus	12		
ll	Lateral Lemniscus	15, 16, 17	25	34
LL	Nucleus of the Lateral Lemniscus	15, 16, 17	24, 25	34
LLD	Nucleus of the Lateral Lemniscus, dorsal part		25, 26	34
LLV	Nucleus of the Lateral Lemniscus, ventral part			34
LoC	Locus Coeruleus	16	25, 26	33, 34
lot	Lateral Olfactory Tract	4, 5	26, 27	34, 35
LOT	Nucleus of the Lateral Olfactory Tract	5, 6, 7	26, 27	34, 35
LPO	Lateral Preoptic Area	8		32
LPR	Lateral Pallium, Rostral Part	4		
LS	Lateral Septal Nucleus	7, 8, 9	27	32
LTu	Lateral Tuberal Nucleus	12	22	
LV	Lateral Ventricle	4, 5, 6, 7, 8, 9, 10	26, 27, 28, 29	32, 33, 34, 35
lvesp	Lateral Vestibulospinal Tract	18, 20	25, 26	34
M	Mammillary Nuclei	13		31
m5n	Motor Root of the Trigeminal Nerve	17	25	
m7n	Motor Root of the Facial Nerve		25	
MA	Medial Amygdala	9	25, 26	34
MC	Magnocellular Cochlear Nucleus	18		32
MCx	Medial Cortex	5, 6, 7, 8, 9, 10, 11	28, 29, 30	31, 32, 33, 34, 35
mfb	Medial Forebrain Bundle	7, 8, 9, 10, 11, 12, 13	24, 25, 26	32
MHb	Medial Habenula	10		31
MJC	Medial Juxtacommissural Nucleus	12	26	31
ml	Medial Lemniscus	15, 16, 17, 18, 19, 20	23, 24, 25	31
ML	Molecular Layer of the Cerebellum	15		32
mlf	Medial Longitudinal Fasciculus	13, 14, 15, 16, 17, 18, 19, 20	24, 25, 26, 27	31, 32
MPC	Medial Parvocellular Nucleus	19	27	
MPO	Medial Preoptic Area	8, 9	25	31
MPR	Medial Pallium, Rostral Part		27	32, 33
MRtF	Middle Reticular Formation	17, 18	23, 24, 25	32, 33
MS	Medial Septal Nucleus	9	27	
MT	Medial Thalamic Nucleus	11	25	31
O	Oval Nucleus		26	32
oc	Optic Chiasm	8, 9, 10	22, 23	31, 32
OP	Olfactory Peduncle			31
ot	Optic Tract	9, 10, 11, 12, 13	22, 23, 24, 25, 26, 27	32, 33, 34
OT	Optic Tectum	11, 12, 13, 14, 15	25, 26, 27, 28, 29, 30	31, 32, 33, 34, 35, 36
p1Tg	p1 Tegmental Area (former Pretectal Reticular Formation, PtR)	13,	25	32, 33, 34
p3Tg	p3 Tegmental Area	12	24	32

TABLE 1 (Continued)

Abbreviation	Brain Region	Coronal Figures	Horizontal Figures	Sagittal Figures
p8n	Posterior Root of the Statoacoustic Nerve	18	26, 27	
Pa	Paraventricular Nucleus	9	24	
PaO	Paraventricular Organ	12	23	31
PaON	Paraventricular Organ Nucleus (formerly Periventricular Hypothalamic Nucleus)	11, 12	23, 24	
PB	Parabrachial Nucleus	15		
pc	Posterior Commissure	12	26, 27	31, 32
PC	Nucleus of the Posterior Commissure	11	26	32
PCN	Posterior Cochlear Nucleus	18		
PCt	Posterocentral Nucleus	11, 12		33
PDN	Posterodorsal Nucleus	12	27	32
pdt	Predorsal Tract	14, 15, 16, 17, 18, 19, 20	24, 25	31
PDVR	Posterior Dorsal Ventricular Ridge	9, 10	27, 28	32, 33
PH	Posterior or Basal Hypothalamus	12	24	
PL	Purkinje Layer of the Cerebellum	15		32
PM	Profound Mesencephalic Area	13, 14	26	34
PMN	Posteromedial Nucleus	11, 12		31, 32
ppc	Posterior Pallial Commissure	10	27	31, 32
PrPC	Principal Precommissural Nucleus	11, 12	25	32
PT	Pallial Thickening	5		
PTE	Prethalamic Eminence		25	32
PTG	Pretectal Geniculate Nucleus	11, 12	25, 26	33, 34
PVSC	Posterior Nucleus of the Ventral Supraoptic Commissure	12	24	34
R	Red Nucleus	14		32
r1Tg	r1 Tegmental Area (Reticular Isthmal Nucleus)	15	25	33
RM	Retromammillary Nucleus	13	23	31
rmc	Retromammillary Commissure	13	23	31
Rot	Rotund Nucleus	11	25	31, 32
S	Septum	5, 6		
s5n	Sensory Root of the Trigeminal Nerve	17		34
s7n	Sensory Root of the Facial Nerve	17	26	
SAT	Striatoamygdaloid Transition Area	8, 9	25, 26, 27	33, 34
SCh	Suprachiasmatic Nucleus	9	24	31
SCO	Subcommissural Organ	12	26	31
SD	Nucleus of the Supraoptic Decussation	11	23	33
sh	Septohypothalamic Tract	9, 10, 11	24, 25, 26	32
sm	Stria Medullaris	9, 10	25	32
SN	Substantia Nigra		25	33, 34
SO	Superior Olivary Nucleus	17	24	33
Sol	Nucleus of the Solitary Tract	19, 20		
sol	Solitary Tract	17, 18	26, 27	
SON	Supraoptic Nucleus	8, 9	24	32
sox	Supraoptic decussation		23	
spce	Spinocerebellar Tract	16, 17, 18	26, 27	34
Sph	Spherical Nucleus	9, 10	25, 26	35
spl	Spinal Lemniscus	15, 16, 17, 18, 19, 20	24, 25, 26, 27	32, 33, 34
SR	Superior Raphe Nucleus	15, 16	23, 24	31
SRtF	Superior Reticular Formation	15, 16	23, 24, 25	32, 33
SRtL	Superior Reticular Area, lateral part	16		
SRtM	Superior Reticular Area, medial part	16		32
STL	Bed Nucleus of the Stria Terminalis, lateral part	9		

TABLE 1 (Continued)

Abbreviation	Brain Region	Coronal Figures	Horizontal Figures	Sagittal Figures
STM	Bed Nucleus of the Stria Terminalis, medial part	9	26	33
T	Triangular Area	10		32
tbd	Tectobulbar Tract, dorsal part	13, 14	26, 27	32, 33
tbv	Tectobulbar Tract, ventral part	14	26	
tc	Tectal Commissure	12, 13	27	31, 32, 33
TG	Tectal Grey	11, 12	26, 27	33, 34
tgd	Tegmental Decussation		24	
TSC	Torus Semicircularis, central nucleus	13, 14, 15	27, 28	31, 32
TSL	Torus Semicircularis, laminar nucleus	13	27	32, 33, 34
tt	Tectothalamic Tract			31
ttc	Tect-tegmental Commissure	14		
Tu	Olfactory Tubercle	4	25	31, 32
TuL	Olfactory Tubercle, lateral part	5, 6		
TuM	Olfactory Tubercle, medial part	5, 6		
TV	Tectal Ventricle	12, 13	27, 28, 29	32, 33, 34, 35
TVe	Tangential Vestibular Nucleus	18		
TZ	Nucleus of the Trapezoid Body	18	24	32
VA	Ventral Amygdala	9		35
vece	Vestibulocerebellar Fibres	17, 18	26, 27	32
VH	Ventral Horn of the Spinal Cord	21		31
VIRtF	Ventral Nucleus of the Inferior Reticular Formation	19, 20	24, 25, 26, 27	32, 33
VL	Ventrolateral Thalamic Nucleus	10, 11	24	
VLS	Ventrolateral Septal Nucleus	8	26	32
VLVe	Ventrolateral Vestibular Nucleus	18	26	32, 33, 34
VM	Ventromedial Thalamic Nucleus	11	24	32
VMH	Ventromedial Hypothalamic Nucleus	11, 12, 13	22	31, 32
VMS	Ventromedial Septal Nucleus	7	26	31
VMVe	Ventromedial Vestibular Nucleus	18		
VP	Ventral Pallidum	7, 8		
VPT	Ventral Pretectal Nucleus	12, 13	25	
VTA	Ventral Tegmental Area	14	24	31
Z	Nucleus Z	12		

the constructed model, using the MINC toolkit (Vincent et al., 2016), and manual corrections. The linear rotational component of the automatic registration was used to measure the angle of alignment of the brain in the skull with respect to our model.

No description exists for the tawny dragon brain or for any agamid brain. A variety of neuroanatomical references available for other lizards (including lacertids, iguanids, and varanids) were used to identify brain areas, including neuroanatomical references for the entire lizard brain (Del Corral, Miralles, Nicolau, Planas, & Rial, 1990; ten Donkelaar, 1998; Medina, Marti, Artero, Fasolo, & Puelles, 1992), the telencephalon (Greenberg, 1982; Northcutt, 1967; Peterson, 1981; Smeets, Hoogland, & Lohman, 1986), the diencephalon (Butler & Northcutt, 1973; Cruce, 1974), the hindbrain (Cruce & Newman, 1981; ten Donkelaar, Bangma, Barbas-Henry, Huizen, & Wolters, 2012; Schwab, 1979; Wolters, ten Donkelaar, & Verhofstad, 1984; Wolters, ten Donkelaar, Steinbusch, & Verhofstad, 1985), and the neuromeric domains (Díaz, Yanes, Trujillo, & Puelles, 2000; Medina, Smeets, Hoogland, & Puelles, 1993; Medina, Puelles, & Smeets, 1994). Another important reference is the turtle brain atlas (Powers & Reiner, 1980).

3 | RESULTS

The tawny dragon brain model described here can be viewed online and downloaded in NIFTI format from wiley.biolucida.net. The model represents the spatial positioning and intensity of each neural structure based on the nonlinear averaging of thirteen tawny dragon brains. Using the intrinsic three-axis nature of MRI-atlases (Ullmann, Cowin, Kurniawan, & Collin, 2010b), we established a coordinate system with *x*-coordinates running medio-laterally, *y*-coordinates running rostro-caudally, and *z*-coordinates running ventro-dorsally, as per convention (Figure 3). The midline of the brain, which divides the two hemispheres, has been designated as the plane $x = 0$. The center of the epiphysis (defined as the *y* plane in which the diameter of the epiphysis reaches its maximum) has been designated as the point $(x,y) = (0,0)$, following

studies which use the parietal eye as the point (*x*,*y*) = (0,0) (Greenberg, 1982). The plane *z* = 0 is located centrally as defined by the dimensions of the image: there are an equal number of z-planes above and below *z* = 0. By convention, *y*-values increase caudally and *z*-values increase dorsally. The model is bilaterally symmetric about the midline, therefore the positive and negative directions in the x-plane are arbitrary.

Our model can be matched to novel MRIs, in vivo or ex vivo, and of different preservation and scanning parameters. This process, called model-based segmentation, is commonly used in medical MRI research (e.g., see Friedel, van Eede, Pipitone, Chakravarty, & Lerch, 2014) and could be easily implemented in evolutionary neuroscience to, for example, digitally "extract" lizard brains from the surrounding tissue in an MRI. We registered our model to a representative MRI scan of an intact tawny dragon head, scanned ex-vivo, to demonstrate the position of the brain (Figure 2a,b). During the registration process, we observed that our atlas is not in the natural orientation of the tawny dragon brain; it is rotated by 28° in the x-plane (Figure 2c). The tawny dragon head MRI is also available for viewing and download from wiley.biolucida.net.

From our atlas, we were able to identify over 200 structures including areas, nuclei, fibre tracts and ventricles (Table 1). Whenever possible, the terminology of ten Donkelaar (1998) was used. Abbreviations follow the standard nomenclature rules as described in the brain atlases co-authored by George Paxinos (e.g., Paxinos & Franklin, 2013; Paxinos & Watson, 2013). Figures 4–20 show our atlas in sequential coronal sections, and we also include a coronal section of the anterior spinal cord (Figure 21). Figures 22–30 show our atlas in sequential horizontal sections, and Figures 31–36 in sequential sagittal sections. Figures 4-36 are presented at the end of this article, after the references, as is traditional for atlases and for ease of use. Higher resolution versions of the atlas figures are freely available from wiley.biolucida.net. The morphology of the dragon brain in our MRI model closely matches coronal nuclear-stained histological sections (Figures 37–45) and therefore our atlas is also relevant for work using traditional neuroanatomical methods.

We have identified the major anatomical divisions of our atlas according to the columnar (Table 2) and neuromeric (Table 3) models. The boundaries between neuromeres are often seen as transverse, dark strips separating grisea. They sometimes run parallel to major fiber tracts, such as the fasciculus retroflexus (adjacent to the boundary between prosomeres 1 and 2), facilitating their visualization. In our model, the three prosomeres of the diencephalon are clearly visible in both coronal and sagittal sections (Figure 46). The divisions between the commonly used columnar regions are not easily distinguished, likely because these regions are artificial; however, we have outlined them for comparative purposes (Figure 46).

In typical MRI images of biological tissue, the signal intensity mainly reflects water content. Since we used a T2*-weighted gradient echo, regions with higher water content appear hyperintense, or close to white in shade. Regions that have low water content appear hypointense, closer to black. The brain regions that have the highest water content are generally regions with high concentrations of cell bodies and/or neuropil and these therefore appear lightest. Fiber tracts tend to be the darkest due to extensive hydrophobic myelination. Nonetheless, in all tissue types signal intensity can vary extensively due to differences in cell size, extent of myelination, and neurochemistry. Signal intensity can even show a gradient within a single region, for example input from the lateral forebrain bundle creates an intensity gradient within the anterior dorsal ventricular ridge (Figure 7). Therefore, different nuclei and fiber tracts are differentiated based not only on differences in signal intensity but also by careful comparison with histological preparations and published literature.

The precise localization of the ventricles is important for identifying surrounding tissue regions, however these structures are particularly difficult to delineate in our atlas. Some ventricles, such as the rostral part of the lateral and tectal ventricles, are filled with aqueous liquid and appear white (e.g., Figures 4, 12–13). Ventricles which have collapsed during perfusion and fixation, and so do not contain any liquid, appear as thin lines of slightly lighter intensity. The majority of the lateral ventricle appears this way (e.g., Figure 7). The third and

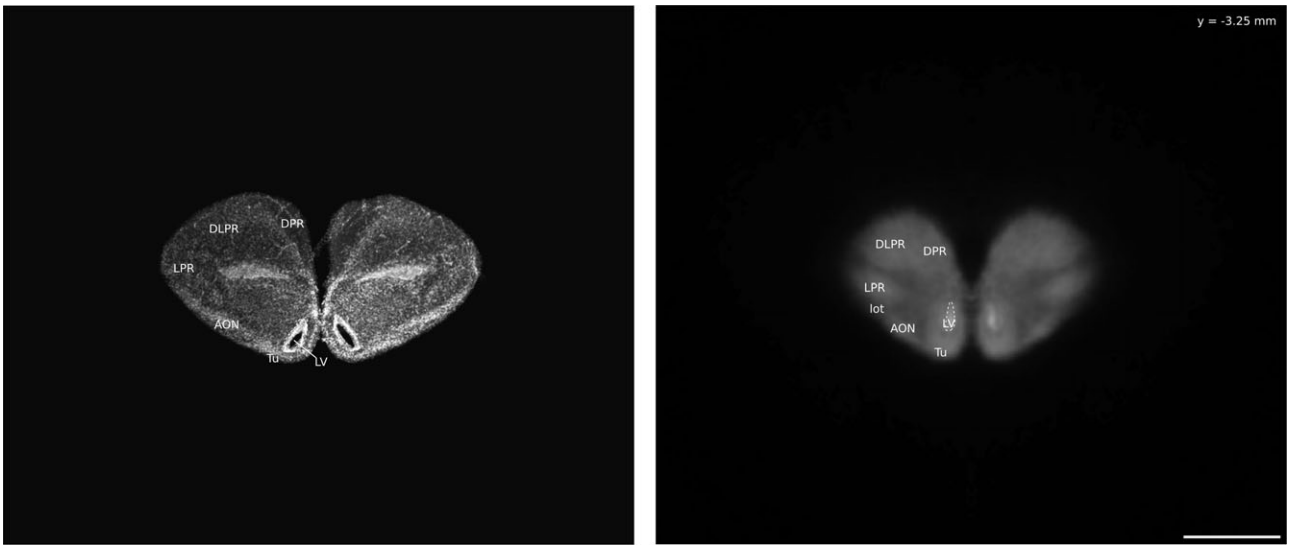

FIGURE 37 A coronal histological section (left panel) of a nuclear-stained anterior telencephalic section of a tawny dragon (*Ctenophorus decresii*) brain demonstrates similar anatomical features to an equivalent section through the MRI model (right panel). The plane according to our coordinate system is indicated in the upper right corner. The scale bar = 1 mm. A list of abbreviations is found in Table 1

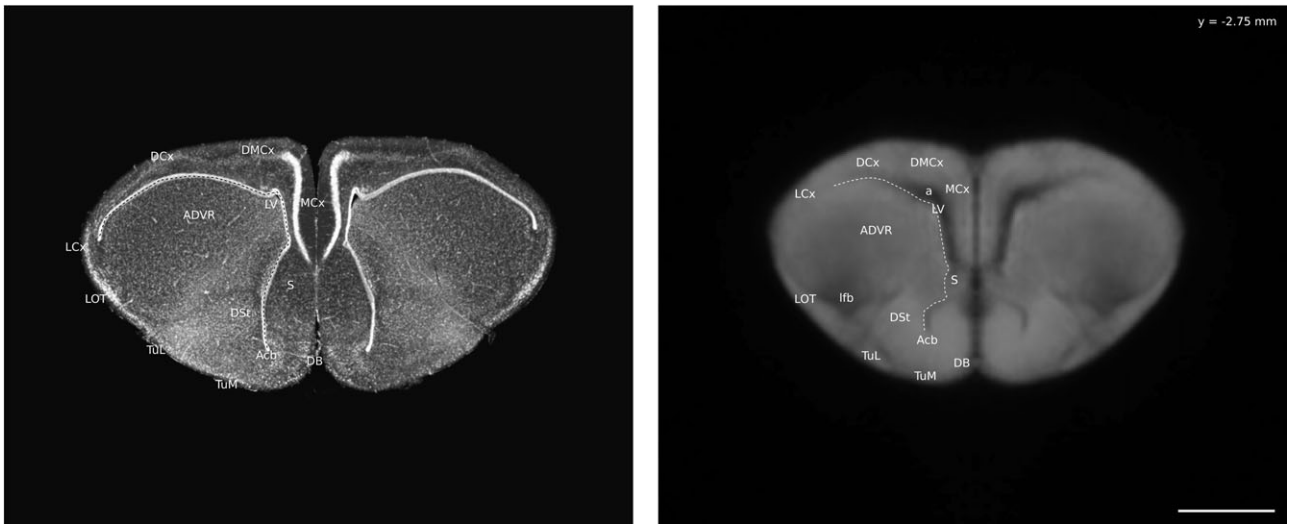

FIGURE 38 A coronal histological section (left panel) of a nuclear-stained mid-telencephalic section of a tawny dragon (*Ctenophorus decresii*) brain demonstrates similar anatomical features to an equivalent section through the MRI model (right panel). The plane according to our coordinate system is indicated in the upper right corner. The scale bar = 1 mm. A list of abbreviations is found in Table 1

fourth ventricles appear black as they have filled with Fomblin, the oil used to immerse the brain during imaging (e.g., Figure 16). Because of this variation, we have outlined ventricles with white dashed lines.

The laminar morphology of some brain regions is readily distinguishable in our atlas, particularly in the cerebral cortex, optic tectum and cerebellum. These layers are not as apparent in the individual MRIs used to make the model, as the differences in intensity are too weak. Only by generating the minimum deformation model from 13 MRIs is the noise reduced, the contrast enhanced, and the layers easily observed. The cerebral cortex generally contains three layers, a main or central cell layer flanked by two plexiform layers. The outer and inner plexiform layers appear relatively light, while the central cell layer appears either lighter or darker than the plexiform layers, depending on cortical area (Figure 47a; also see next paragraph). The darkest layer is the alveus that runs deep within the inner plexiform layer and is continuous with the anterior and posterior pallial commissures. A cell layer, the periventricular layer, exists along the surface of the lateral ventricle, but is not distinguishable from the alveus in our model.

The cerebral cortex is divisible into four main areas, which are distinguishable based on their relative positions and the morphology of the central cell layer. The medial cortex lies above the septum and is characterized by a cell layer that is distinctly darker than the surrounding plexiform layers. In the dorsomedial cortex, the cell layer widens, becomes lighter in intensity and appears slightly convex. An additional cell layer, the cell plate of the inner plexiform layer of the dorsomedial cortex, is visible in the inner plexiform layer. The dorsal cortex shows the distinct three-layered structure with a thin, prominent cell layer anteriorly that becomes less distinct as the inner plexiform layer decreases in intensity posteriorly. The lateral cortex is the most indistinct because its cell layer is diffuse and provides little contrast to the plexiform layers.

The reptilian optic tectum has a marked laminar organization consisting of cell layers separated by fiber layers; in some reptiles a total

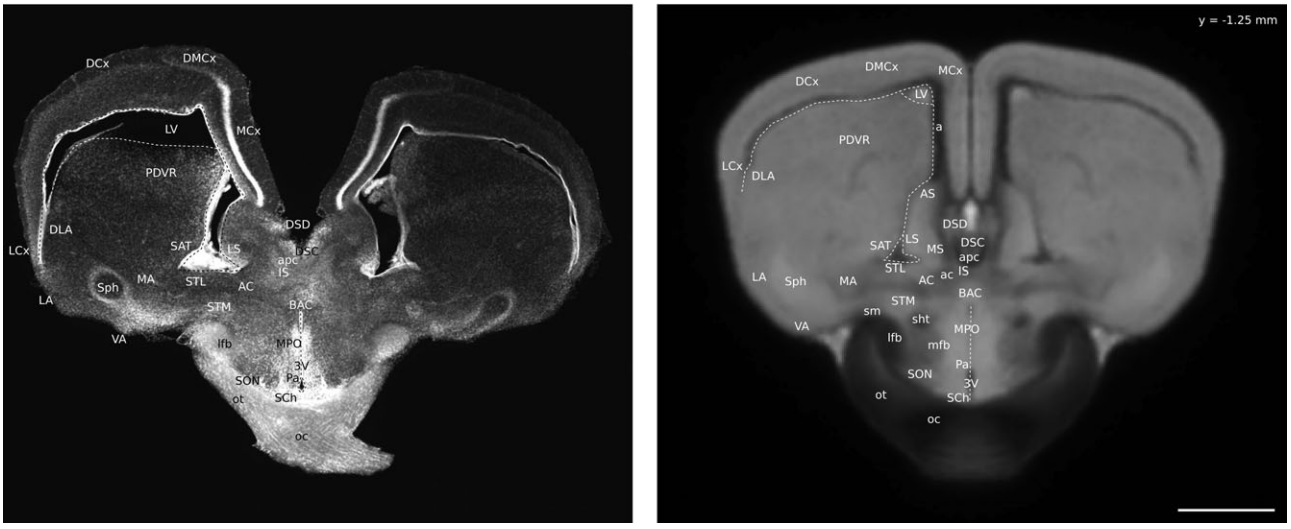

FIGURE 39 A coronal histological section (left panel) of a nuclear-stained posterior telencephalic section of a tawny dragon (*Ctenophorus decresii*) brain demonstrates similar anatomical features to an equivalent section through the MRI model (right panel). The plane according to our coordinate system is indicated in the upper right corner. The scale bar = 1 mm. A list of abbreviations is found in Table 1

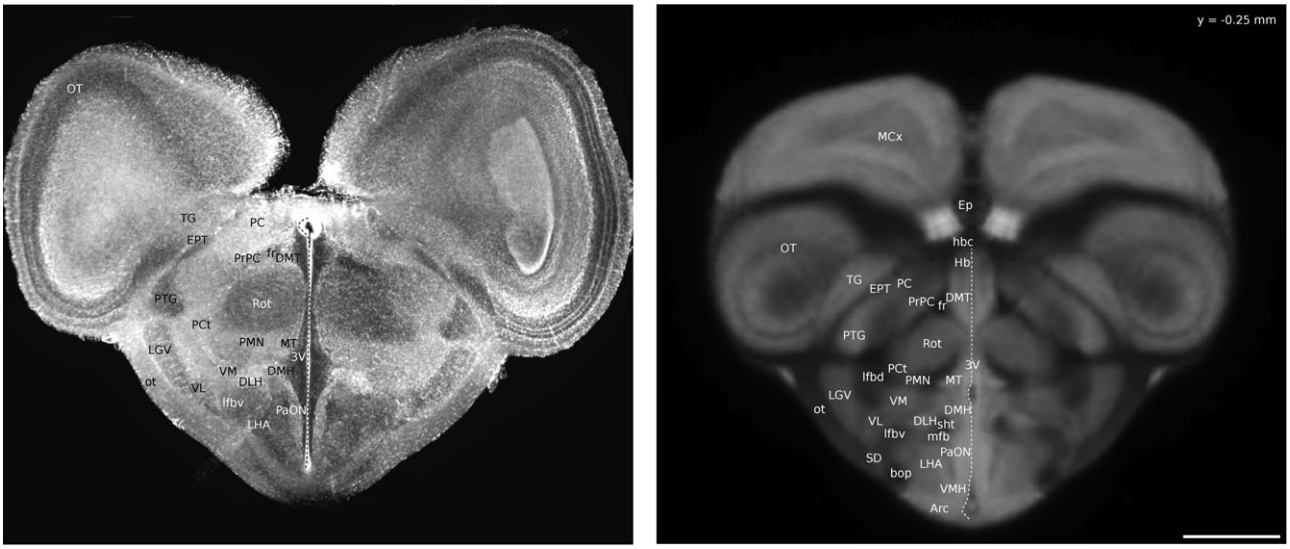

FIGURE 40 A coronal histological section (left panel) of a nuclear-stained anterior diencephalic section of a tawny dragon (*Ctenophorus decresii*) brain demonstrates similar anatomical features to an equivalent section through the MRI model (right panel). The plane according to our coordinate system is indicated in the upper right corner. The scale bar = 1 mm. A list of abbreviations is found in Table 1

of fourteen layers have been described (Ramón, 1891). These have been grouped in six main layers or strata (ten Donkelaar, 1998), which are readily distinguishable in our model (Figure 47b). The optical layer is only slightly darker than the adjacent superficial grey and fibrous layer, but the two can be distinguished by the dark border between them. The central white layer is the darkest layer, while the central grey layer is of intermediate intensity between the central white and superficial layers. The periventricular grey layer is darker than the superficial layers but lighter than the central white layer, and finally the periventricular white layer is as dark as the central white layer, but much thinner (Figure 47b).

It is also possible identify the three layers of the cerebellum: the outer molecular layer, the central Purkinje layer, and the inner granular layer (Figure 47c). In lizards, including the tawny dragon, the cerebellum is everted (ten Donkelaar & Bangma, 1992). The Purkinje layer is the darkest in our MRI, likely owing to the fact that this layer contains not only the big somas of the Purkinje cells, but also a band of primarily afferent fibers. The granular layer is the lightest in intensity.

Not all structures visible in our MRI model are made up of neural tissue. In the anterior dorsal ventricular ridge, some arteries can clearly be seen as a series of dark spots (Figure 8; indicated by an asterisk). The meninges can be seen as thin, light structures around the edge of the brain, particularly in images of the brain stem (e.g., Figure 17). Droplets of the aqueous storage solution can get trapped around the brain when transferring them to Fomblin for imaging. These appear as bright areas in some images, for example the spaces between the optic tectum and the epiphysis (Figure 12) and between the optic tectum and the cerebellum (Figure 14).

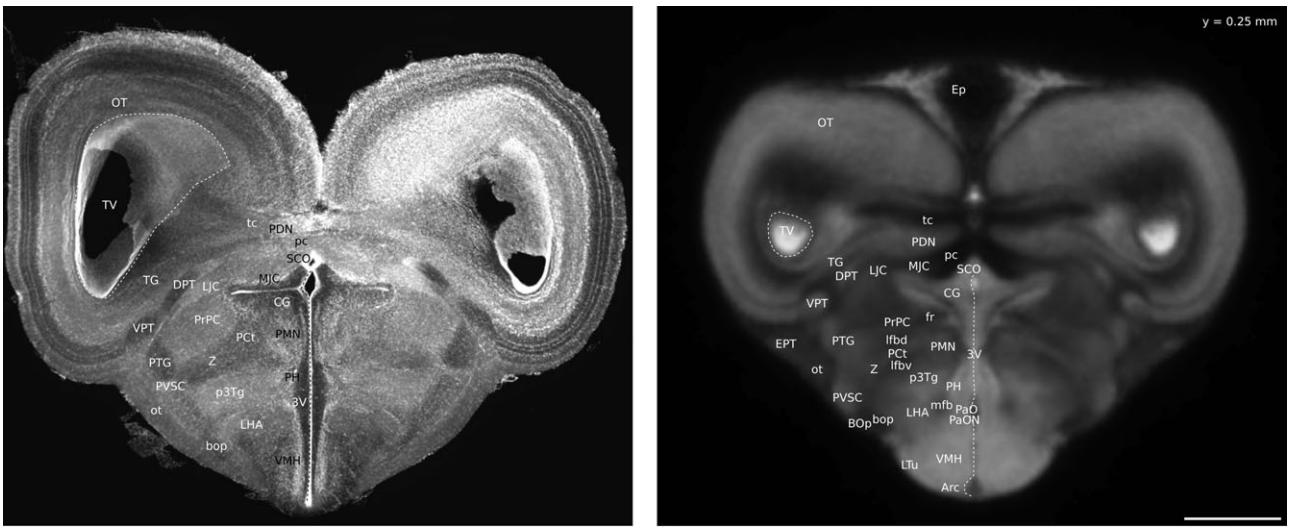

FIGURE 41 A coronal histological section (left panel) of a nuclear-stained mid-diencephalic section of a tawny dragon (*Ctenophorus decresii*) brain demonstrates similar anatomical features to an equivalent section through the MRI model (right panel). The plane according to our coordinate system is indicated in the upper right corner. The scale bar = 1 mm. A list of abbreviations is found in Table 1

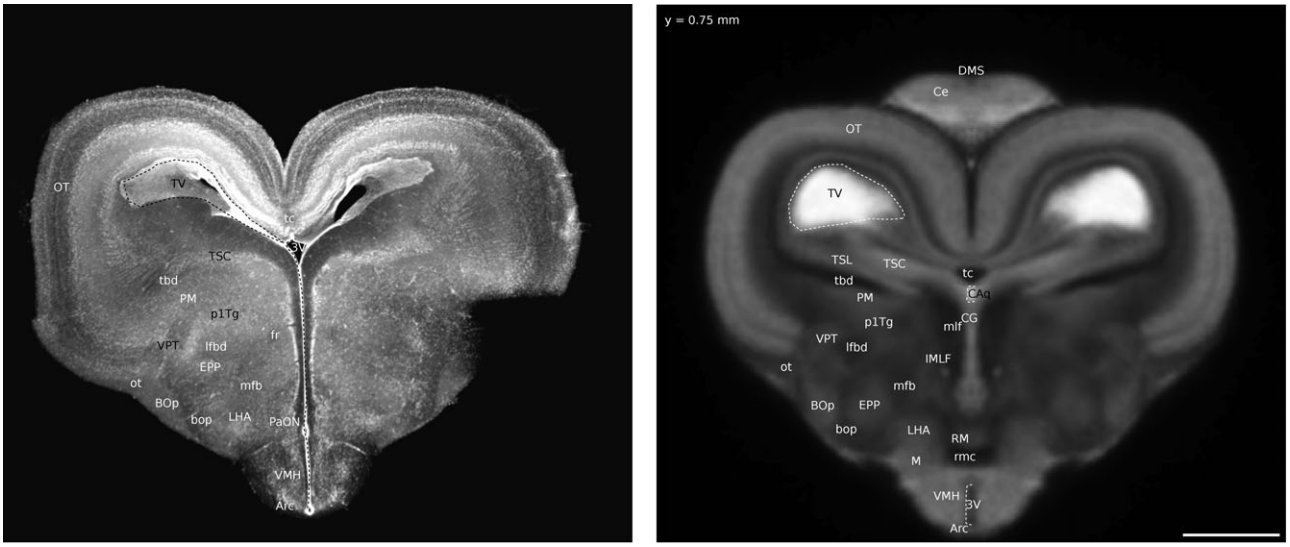

FIGURE 42 A coronal histological section (left panel) of a nuclear-stained posterior diencephalic section of a tawny dragon (*Ctenophorus decresii*) brain demonstrates similar anatomical features to an equivalent section through the MRI model (right panel). The plane according to our coordinate system is indicated in the upper right corner. The scale bar = 1 mm. A list of abbreviations is found in Table 1

4 | DISCUSSION

4.1 | MRI as a method for studying comparative neuroanatomy

To create an atlas with the best possible resolution, we have used a non-linear image averaging strategy to create an 'idealized' model of a tawny dragon brain (Janke & Ullmann, 2015). The model represents a significant improvement in resolution over the MRIs of individual brains (Figure 1), and this technique is now a standard component of the image registration process for modern structural MRI analysis (Johnson, Calabrese, Badea, Paxinos, & Watson, 2012; Maldjian, Daunais, Friedman, & Whitlow, 2014; Ullmann, Watson, Janke, Kurniawan, & Reutens, 2013a).

Unlike histology, in MRI brain size impacts the level of discernable detail. For example, an MRI atlas of a monkey brain is able to delineate 720 structures in an image with a 0.5 mm^3 voxel size (Maldjian, Daunais, Friedman, & Whitlow, 2014), whereas an MRI atlas of a cichlid brain is able to delineate only 54 structures in an image with a 50 μm^3 voxel size (Simões, Teles, Oliveira, Van der Linden, & Verhoye, 2012). Though the absolute voxel size in the cichlid atlas is much smaller than the voxel size in the monkey atlas, voxel size relative to brain size is much smaller in the monkey atlas. This provides a two-fold benefit to the monkey atlas: the larger absolute voxel size provides greater signal intensity, while smaller relative voxel size provides greater spatial resolution. Together, these factors allow for much more precise structural delineation in larger brains. This is an important consideration for comparative neuroscience, where comparisons are often made

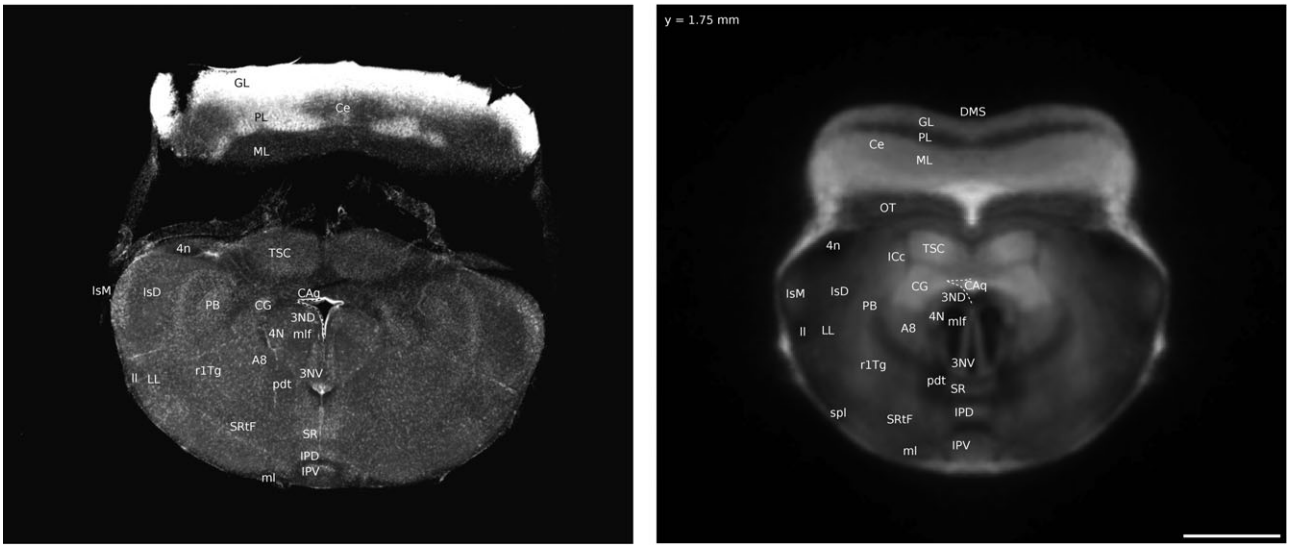

FIGURE 43 A coronal histological section (left panel) of a nuclear-stained anterior rhombencephalic section of a tawny dragon (*Ctenophorus decresii*) brain demonstrates similar anatomical features to an equivalent section through the MRI model (right panel). The plane according to our coordinate system is indicated in the upper right corner. The scale bar = 1 mm. A list of abbreviations is found in Table 1

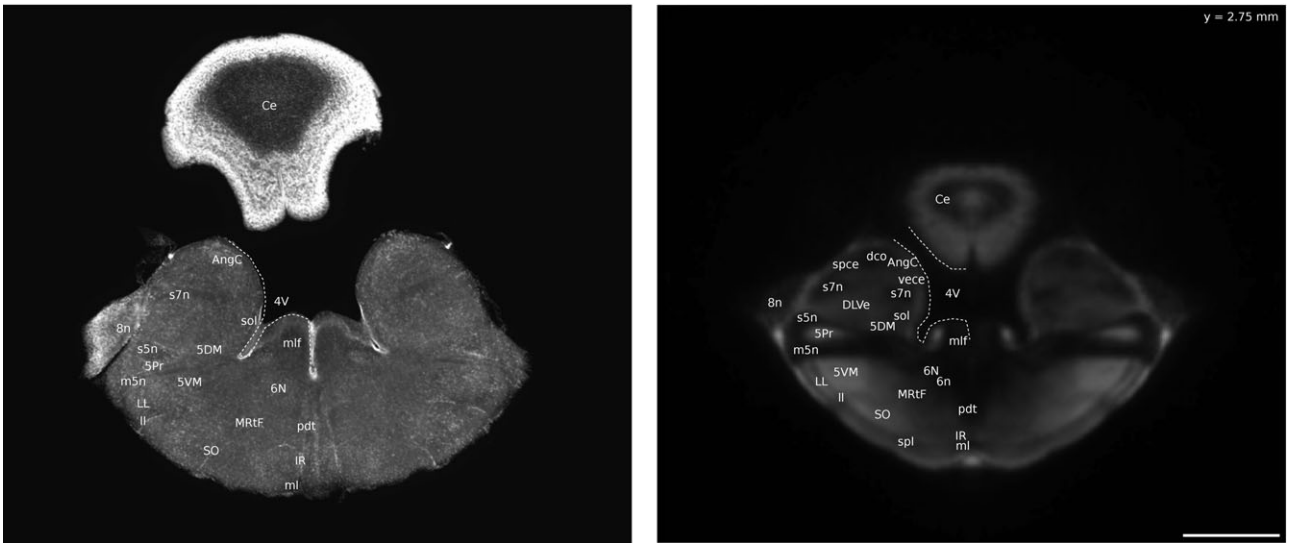

FIGURE 44 A coronal histological section (left panel) of a nuclear-stained mid-rhombencephalic section of a tawny dragon (*Ctenophorus decresii*) brain demonstrates similar anatomical features to an equivalent section through the MRI model (right panel). The plane according to our coordinate system is indicated in the upper right corner. The scale bar = 1 mm. A list of abbreviations is found in Table 1

between brains that differ in size by orders of magnitude. Using multiple MRIs to create a non-linear average brain model can help offset these issues in species with small brains.

4.2 | The columnar and neuromeric models of brain organization

The study of brain structure requires a model of brain organization that sets easily recognized landmarks that help identify neural structures along pre-established axes (Puelles, 2009). In these models, the relative topological positions of the brain divisions should be invariant, independent of differences in size and shape arising through development or evolution (Nieuwenhuys & Puelles, 2015; Nieuwenhuys, ten Donkelaar, & Nicholson, 1998). Two models are currently used to interpret brain morphology, the columnar and neuromeric/prosomeric models.

The columnar model of neural divisions has been the predominant model of the second half of the twentieth century. It was based on the discovery of distinct functional columns in the spinal cord, the alar plate or dorsal horn and the basal plate or ventral horn. The model was then applied to the brain (Herrick, 1910; reviewed by Puelles, 2009). Thus, the diencephalon was described as containing several dorsoventral columns, including epithalamus, dorsal thalamus, ventral thalamus and hypothalamus. This description is still used by many neuroscientists and is found in the majority of textbooks. However, the columnar model is increasingly being recognized as unnatural

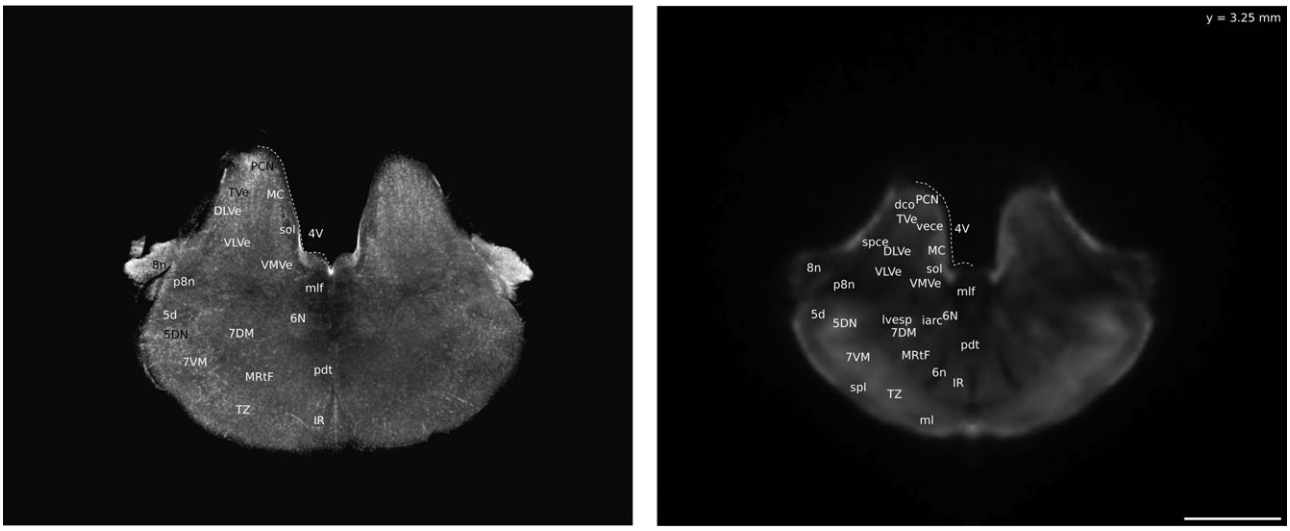

FIGURE 45 A coronal histological section (left panel) of a nuclear-stained posterior rhombencephalic section of a tawny dragon (*Ctenophorus decresii*) brain demonstrates similar anatomical features to an equivalent section through the MRI model (right panel). The plane according to our coordinate system is indicated in the upper right corner. The scale bar = 1 mm. A list of abbreviations is found in Table 1

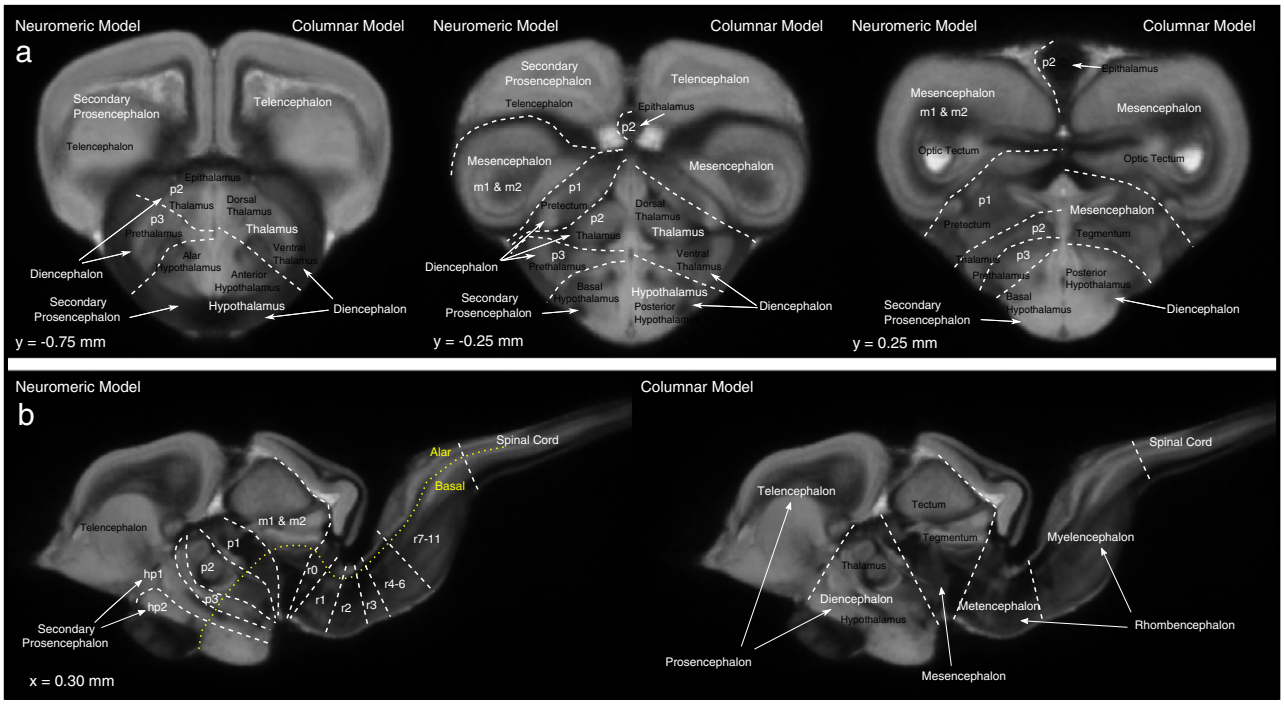

FIGURE 46 The divisions of the lizard brain according to different models of brain organization. We have delineated the major neural subdivisions according to both the neuromeric and columnar models of brain organization in (a) selected coronal sections and (b) a sagittal section to demonstrate how these different models partition the brain. White text labels the major rostro-caudal neural subdivisions, which are delineated by broken white lines. Yellow text labels the major dorso-ventral neural subdivisions, which are delineated by broken yellow lines. Black text labels commonly used minor regional designations within the major subdivisions. The plane of each section according to our coordinate system is indicated in the lower left corner. hp = hypothalamic prosomere, m = mesomere, p = prosomere, r = rhombomere [Color figure can be viewed at wileyonlinelibrary.com]

because it does not consider the curvature of the longitudinal brain axis and the true morphogenetic divisions specified during development (reviewed by Puelles, 2009).

The neuromeric model (called the prosomeric model when discussing the forebrain) was employed by neuroembryologists during late nineteenth and early twentieth centuries, and was based on the periodic transversal bulges (called neuromeres) in the neural tube wall during embryonic development (Kupffer, 1906; Orr, 1896; Puelles, 2009; Puelles et al., 2013). This model has recently experienced a resurgence due to its suitability for explaining the expression patterns of developmental regulatory genes and their mutant phenotypes, the results of experimental studies such as transplants and fate mappings, and the trajectories of major fiber tracts (Díaz & Glover, 2002; Marín & Puelles, 1995; Martínez, Marín, Nieto, & Puelles, 1995; Puelles, 2009; Puelles et al., 2013; Puelles & Rubenstein, 1993,2003; Shimamura, Hartigan, Martínez, Puelles, & Rubenstein, 1995). The model is already applied in widely used brain atlases, such as the last edition of the rat brain atlas (Paxinos & Watson, 2013), the Allen Developing Mouse Brain Atlas (http://developingmouse.brain-map.org/), and the chicken brain atlas (Puelles, Martínez-de-la-Torre, Paxinos, Watson, & Martinez, 2007). It is starting to be incorporated into MRI atlases (Watson et al., 2017).

The neuromeric model is powerful for comparative purposes since the same developmental units are found in all vertebrates (Medina, 2006; Puelles et al., 2007; Puelles & Medina, 2002). For these reasons, in this study we used the neuromeric model as our preferred paradigm to interpret MRI data, with the hope that this will be more useful for future functional and evolutionary studies using our atlas. The boundaries between neuromeres were identified as dark transversal strips (i.e., thin, cell poor areas) between grisea (which appear lighter). Fiber tracts, easily followed in our 3D atlas, are also useful for understanding the neuromeric organization of the tawny dragon brain, as their main trajectories are often either longitudinal (i.e., parallel to the alar-basal boundary) or transverse (i.e., parallel to the divisions between neuromeres). Though this model is based on the natural divisions of the brain and therefore is more desirable than the columnar model, the columnar model remains dominant in everyday use. Therefore, we provide Table 2, Table 3, and Figure 46 comparing the major brain divisions and subdivisions according to each model. The major differences occur in the forebrain, due to the different interpretation of the longitudinal (rostrocaudal) axis and, consequently, opposite view of the transverse (dorsoventral) divisions.

4.3 | Comparison with other squamates

Although all lizards share a basic pattern of brain organization, there are divergences in morphology that are related to the widespread morphological, ecological, and behavioral differences between species. For instance, the optic tectum is larger in diurnal lizards than in nocturnal ones, and the size of the cerebellum is related to the type of locomotion, being smaller and simpler in limbless than quadrupedal lizards (Dacey & Sereno, 1992; ten Donkelaar, 1998; ten Donkelaar & Bangma, 1992; Platel, 1976). Both the optic tectum and the cerebellum of the tawny dragon are well developed, as predicted for a

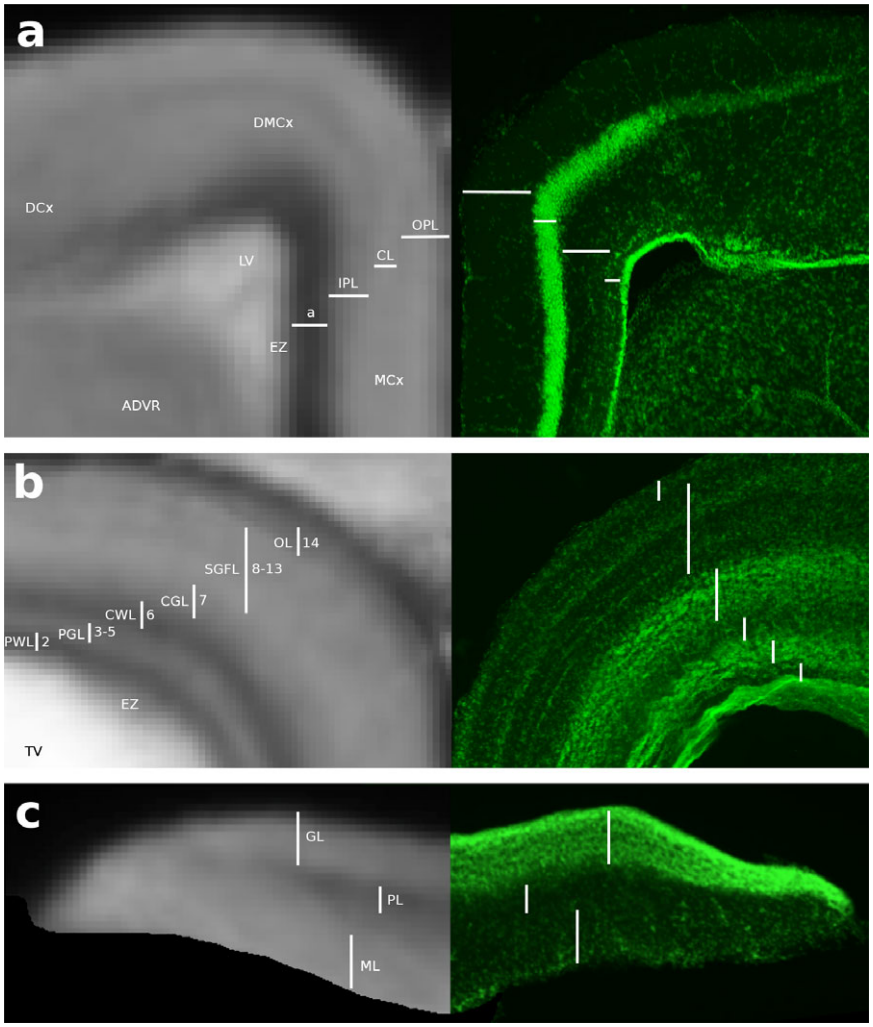

FIGURE 47 Coronal sections through an MRI model (grey scale) and a fluorescent DNA-stained brain (green) compare the appearance of (a) the medial, dorsomedial and dorsal cortices, (b) the optic tectum, and (c) the cerebellum. a = alveus, CGL = central grey layer, CL = cell layer, CWL = central white layer, DCx = dorsal cortex, DMCx = dorsomedial cortex, EZ = ependymal zone, GL = glomerular layer, IPL = inner plexiform layer, LV = lateral ventricle, MCx = medial cortex, ML = molecular layer, OL = optic layer, OPL = outer plexiform layer, PGL = periventricular grey layer, PL = Purkinje layer, PWL = periventricular white layer, SGFL = superficial grey and fibrous layer, TV = tectal ventricle [Color figure can be viewed at wileyonlinelibrary.com]

quadrupedal diurnal lizard (Gibbons, 1979; Osborne, Umbers, & Keogh, 2013; Osborne, Umbers, Backwell, & Keogh, 2012).

In the tawny dragon, we have identified the four classical cortical areas of the lizard brain: the medial, dorsomedial, dorsal, and lateral cortices (Striedter, 1997). In the dorsomedial cortex there is a cell plate visible in the inner plexiform layer (the CPDMCx in Figure 10), close to the ventricle and associated with a small but distinct ventricular ridge and a thickening of the overlying dorsomedial cortex. A similar organization is also observed in *Agama agama* (Figure 1B of Wouterlood, 1981). In other lizards, this inner cell plate is not as evident, although some cell clusters can be observed in a similar position (Martinez-Guijarro, Desfilis, & Lopez-Garcia, 1990; Medina et al., 1992; Smeets et al., 1986). In gekkonids, lacertids, and iguanids, the cell clusters are more numerous in the inner plexiform layer of the dorsal cortex instead of the dorsomedial cortex. Some of these form a plate referred as the cell plate of Unger (Lacerta: Medina et al., 1992; Gecko: Smeets et al., 1986) or the supraventricular layer (Iguana: Northcutt, 1967). In the green anole a cell plate is visible in the medial and dorsomedial cortices; Greenberg (1982) labelled it the dorsomedial interposition.

The identification of the dorsal pallium in reptiles has been controversial, for example see Butler (2011) versus Puelles (2006). Based on genoarchitecture during development, Desfilis *et al*. (2018) proposed that it is located in a very rostral and medial position, resembling that of the avian dorsal pallium, or Wulst. This area shows a different cytoarchitecture compared to medial, dorsomedial and dorsal cortices, which appear more caudally (Desfilis et al., 2018). In our MRI atlas, we identified this dorsal pallial area at very rostral telencephalic levels and accordingly named it rostrodorsal pallium (DPR; Figures 4, 37a). At these very rostral levels we have also identified other pallial divisions: the dorsolateral pallium (DLPR), the lateral pallium (LPR), medial pallium (LPM), and the ventral pallium (including the anterior olfactory nucleus, AO).

The dorsal ventricular ridge, a structure unique to sauropsids, is likely derived from two pallial divisions: most of it belongs to the ventral pallium, while its caudolateral pole belongs to the ventrocaudal

TABLE 2 The principal rostrocaudal and dorsoventral subdivisions of the central nervous system according to the columnar model of neural divisions. The dorsoventral subdivisions of roof and floor, which are universally present, are omitted

Primary rostrocaudal subdivisions	Secondary rostrocaudal subdivisions	Primary dorsoventral divisions
Prosencephalon or forebrain	Telencephalon	Pallium
		Subpallium
	Diencephalon	Epithalamus
		Dorsal thalamus
		Ventral thalamus
		Hypothalamus
Mesencephalon or midbrain	Mesencephalon or midbrain	Tectum
		Midbrain tegmentum
Rhombencephalon or hindbrain	Metencephalon	Cerebellum
		Pontine tegmentum
	Myelencephalon	Several sensory nuclei (such as the nucleus of the solitary tract and the descending trigeminal nucleus)
		Medullar tegmentum
Spinal Cord	Spinal segments	Alar plate/dorsal horn
		Basal plate/ventral horn

pallium (Desfilis et al., 2018). These two sectors of the dorsal ventricular ridge are evident at the caudal telencephalic levels of our atlas (e.g., Figure 10), since they appear as two light areas separated by a dark (i.e., cell poor) strip of tissue. In *Iguana* these two areas are also separated by a cell-poor lamina (Northcutt, 1967). In birds, the corresponding regions are the nidopallium and arcopallium, which are again separated by a cell-poor lamina (Desfilis et al., 2018).

In our model, the most prominent component of the ventrocaudal pallium is the nucleus sphericus, a structure that exhibits substantial variation in size and complexity between species. This nucleus is involved in vomerolfaction and receives massive afferents from the accessory olfactory bulb (Lanuza & Halpern, 1997; Lohman & Smeets, 1993; Martínez-García, Olucha, Teruel, Lorente, & Schwerdtfeger, 1991). The degree of development of this nucleus likely relates to its chemosensory function. In species that use the vomeronasal system extensively, such as snakes and lizards with forked tongues, the spherical nucleus occupies a large proportion of the dorsal ventricular ridge (Cooper, 1995; Halpern, 1980; Schwenk, 1993). In species with a reduced vomeronasal organ, this nucleus may be practically nonexistent, as is the case in *Anolis* (Greenberg, 1982). In the tawny dragon, the spherical nucleus appears to be of intermediate size, similar to *Iguana* (Northcutt, 1967). Both of these species, like *Anolis*, do not have forked tongues and are not thought to be heavily reliant on vomeronasal input. However, unlike *Anolis*, *Ctenophorus* and *Iguana* have femoral pores which produce a waxy substance (Gray, 1827) that is likely used for chemosensory signaling through the vomeronasal system (Baeckens, Edwards, Huyghe, & Van Damme, 2015; Martin & Lopez, 2000).

4.4 | Relevance of the tawny dragon for studies on the neurobiological basis of behavior

Among squamate reptiles, agamids (dragon lizards, Hamilton, May, & Waters, 2015), with more than 300 species, form an enormously diverse group with extensive morphological, ecological, and behavioral differences between species. Agamids are considered a good model for the study of evolutionary biology (Chen, Stuart-Fox, Hugall, & Symonds, 2012; Melville, Ritchie, Chapple, Glor, & Schulte, 2011; Stuart-Fox & Owens, 2003). In particular, the genus *Ctenophorus* has been the object of numerous ecological and behavioral comparative studies (Osborne, 2005a; Stuart-Fox, Moussalli, Johnston, & Owens, 2004; Umbers, Osborne, & Keogh, 2012).

Some tawny dragon populations are color-polymorphic and each morph exhibits different social and reproductive strategies (McLean, Stuart-Fox, & Moussalli, 2014; Teasdale, Stevens, & Stuart-Fox, 2013; Yewers, Pryke, & Stuart-Fox, 2016). Recently, there has been intense interest in studying color polymorphic lizards as models of the origin and maintenance of intraspecific phenotypic and genetic diversity (Corl, Davis, Kuchta, & Sinervo, 2010; McLean & Stuart-Fox, 2014; Vercken, Massot, Sinervo, & Clobert, 2007; Zamundio & Sinervo, 2003). One common finding is variation in reproductive strategy between color morphs (McLean & Stuart-Fox, 2014; Osborne, 2005b, 2005a; Osborne et al., 2012; Teasdale et al., 2013; Wellenreuther, Svensson, & Hansson, 2014; Yewers et al., 2015; Zamundio & Sinervo, 2003). However, little attention has been paid to neural differences between morphs, despite their obvious potential role in driving behavioral variation, including reproductive strategies (but see LaDage et al., 2009,2013). Another *Ctenophorus* species, the painted dragon (*C. pictus*), is also color polymorphic (Healey, 2008; Olsson, Schwartz, Uller, & Healey, 2009; Tobler, Healey, & Olsson, 2011), but most remaining *Ctenophorus* species are monomorphic, making this genus an ideal system for studying the evolution of color polymorphism and its relationship to behavioral and neural variation. Further work using color polymorphic lizard species holds great potential in elucidating the neural underpinnings of different reproductive strategies.

5 | CONCLUSIONS

This is the first time, to our knowledge, that an MRI atlas of a lizard brain has been produced. MRI is an innovative technique used frequently in the medical sciences. Here, we have added the first reptile

TABLE 3 The principal rostrocaudal and dorsoventral subdivisions of the central nervous system according to the neuromeric model of neural subdivisions. The dorsoventral subdivisions of roof and floor, which are universally present, are omitted

Primary rostrocaudal subdivisions	Secondary rostrocaudal subdivisions (protosegments)	Tertiary rostrocaudal subdivisions (segments)	Primary dorsoventral subdivisions	
Prosencephalon or forebrain	Secondary prosencephalon	Terminal or rostral hypothalamic prosomere (hp2)	Alar	Preoptic area Alar terminal hypothalamus
			Basal	Basal terminal hypothalamus
		Peduncular or caudal hypothalamic prosomere (hp1)	Alar	Evaginated telencephalon (pallium and most subpallium) Alar peduncular hypothalamus
			Basal	Basal peduncular hypothalamus
	Diencephalon	Prosomere 3 (p3)	Alar	Prethalamic eminence Prethalamus
			Basal	p3 tegmentum
		Prosomere 2 (p2)	Alar	Epithalamus Thalamus
			Basal	p2 tegmentum
		Prosomere 1 (p1)	Alar	Pretectum
			Basal	p1 tegmentum
Mesencephalon or midbrain	Mesencephalon or midbrain	Mesomeres 1 and 2	Alar	Tectum
			Basal	Tegmentum (III motor nuclei)
Rhombencephalon or hindbrain	Prepontine (Istmo-cerebellar) division	Rhombomeres 0, 1, 2 (r0, r1, r2)	Alar	Isthmic nuclei Locus coeruleus Rostral vestibular nuclei Main trigeminal nucleus Cerebellum
			Basal	IV and V motor nuclei and nerve exits (IV at r0; V at r2)
	Pontine division	Rhombomeres 3, 4 (r3, r4)	Alar	Parts of vestibular nuclei Part of descending trigeminal nucleus
			Basal	V motor nuclei at r3, VII and VIII nerve exits at r4
	Ponto-medullary division	Rhombomeres 5, 6 (r5, r6)	Alar	Parts of vestibular nuclei Part of descending trigeminal nucleus
			Basal	VI motor nucleus and nerve exit at r5, VII motor nuclei at r6
	Medullary division	Rhombomeres 7-11 (r7-r11)	Alar	Parts of vestibular nuclei Part of descending trigeminal nucleus Nucleus of the solitary tract Nuclei of the dorsal column
			Basal	IX, X & XII motor nuclei & nerve exits
Spinal Cord	Cervical, Thoracic, Lumbar, Sacral, Coccygeal regions	Myelomeres	Alar	Dorsal Horn
			Basal	Intermediate and Ventral Horns

to the growing list of MRI atlases available for non-traditional study organisms. The resolution obtained in this atlas is significantly higher than that of other atlases for animals with similarly-sized brains. We hope this atlas provides inspiration to further the study of the reptile brain, the correlation between brain structure and function, and the study of brain evolution, particularly using comparative methods. Only by advancing research in all these fields can we understand the general principles of vertebrate brain organization and identify selective pressures and mechanisms behind variation in the functional organization of the brain. We aspire to develop a range of MRI atlases representing, as much as possible, the diversity of vertebrates. Our goal is to make these universally available through a virtual museum, similar to those provided by brain collections in traditional brick-and-mortar museums (Iwaniuk, 2010,2011), and more recently by the on-line brain collections such as the Comparative Mammalian Brain Collection (http://neurosciencelibrary.org) and BrainMaps.org (http://brainmaps.org/).

6 | DATA ACCESSIBILITY

The MRI model of a tawny dragon brain (*Ctenophorus decresii)*, the dragon brain atlas, and the MRI of a tawny dragon head are freely available for download from the Wiley Biolucida Server at wiley.biolucida.net.

ACKNOWLEDGMENTS

We thank the facilities and the scientific and technical assistance of the National Imaging Facility, Western Sydney University and University of Queensland Nodes. B. Moroney (Nanoscale Group, Western Sydney University) designed the lizard brain holder that made the MRI scanning possible. D.H. was supported by grants from the Government of Australia (APA#31/2011, IPRS#1182/2010), the National Science and Engineering Research Council of Canada (PGSD3-415253-2012), the Quebec Nature and Technology Research Fund (208332), and the

National Imaging Facility of Australia (Subsidized Access Grant). E.D. and L.M. were supported by grants from the Spanish Ministerio de Economía y Competitividad and Fondo Europeo de Desarrollo Regional (BFU2015-68537-R). E.D. and L.M. are Serra Húnter Fellows. M.J.W. and J.S.K. were supported by Australian Research Council Grants DP130102998 and DP150102403 respectively.

REFERENCES

Amiel, J. J., Bao, S., & Shine, R. (2017). The effects of incubation temperature on the development of the cortical forebrain in a lizard. Animal Cognition, 20(1), 117–125. http://doi.org/10.1007/s10071-016-0993-2

Anderson, C. L., Kabalka, G. W., Layne, D. G., Dyke, J. P., & Burghardt, G. M. (2000). Noninvasive high field MRI brain imaging of the garter snake (*Thamnophis sirtalis*). Copeia, 1, 265–269.

Baeckens, S., Edwards, S., Huyghe, K., & Van Damme, R. (2015). Chemical signalling in lizards: an interspecific comparison of femoral pore numbers in Lacertidae. Biological Journal of the Linnean Society, 114(1), 44–57. http://doi.org/10.1111/bij.12414

Butler, A. B., & Northcutt, R. G. (1973). Architectonic studies of the diencephalon of *Iguana iguana* (Linnaeus). The Journal of Comparative Neurology, 149(4), 439–462. http://doi.org/10.1002/cne.901490404

Butler, A. B., Reiner, A., & Karten, H. J. (2011). Evolution of the amniote pallium and the origins of mammalian neocortex. Annals of the New York Academy of Sciences, 1225(1), 14–27. http://doi.org/10.1111/j.1749-6632.2011.06006.x

Chen, I.-P., Stuart-Fox, D. M., Hugall, A. F., & Symonds, M. R. E. (2012). Sexual selection and the evolution of complex color patterns in dragon lizards. Evolution, 66(11), 3605–3614. http://doi.org/10.1111/j.1558-5646.2012.01698.x

Clark, B. F., Amiel, J. J., Shine, R., Noble, D. W. A., & Whiting, M. J. (2013). Colour discrimination and associative learning in hatchling lizards incubated at 'hot' and 'cold' temperatures. Behavioral Ecology and Sociobiology, 68(2), 239–247. http://doi.org/10.1007/s00265-013-1639-x

Cooper, W. E. Jr. (1995). Foraging mode, prey chemical discrimination, and phylogeny in lizards. Animal Behaviour, 50(4), 973–985. http://doi.org/10.1016/0003-3472(95)80098-0

Corfield, J. R., Wild, J. M., Cowan, B. R., Parsons, S., & Kubke, M. F. (2008). MRI of postmortem specimens of endangered species for comparative brain anatomy. Nature Protocols, 3(4), 597–605. http://doi.org/10.1038/nprot.2008.17

Corl, A., Davis, A. R., Kuchta, S. R., & Sinervo, B. (2010). Selective loss of polymorphic mating types is associated with rapid phenotypic evolution during morphic speciation. Proceedings of the National Academy of Sciences, 107(9), 4254–4259. http://doi.org/10.1073/pnas.0909480107

Cruce, J. A. F. (1974). A cytoarchitectonic study of the diencephalon of the tegu lizard, *Tupinambis nigropunctatus*. The Journal of Comparative Neurology, 153(3), 215–238. http://doi.org/10.1002/cne.901530302

Cruce, W. L. R., & Newman, D. B. (1981). Brain stem origins of spinal projections in the lizard *Tupinambis nigropunctatus*. The Journal of Comparative Neurology, 198(2), 185–207. http://doi.org/10.1002/cne.901980202

Dacey, D. M., & Sereno, M. I. (1992). The Optic Tectum. In *Biology of the Reptilia: Sensorimotor Integration*. Vol. 17, pp. 330–366. Chicago, IL: University of Chicago Press.

Day, L. B., Crews, D., & Wilczynski, W. (1999). Relative medial and dorsal cortex volume in relation to foraging ecology in congeneric lizards. Brain, Behavior and Evolution, 54(6), 314–322.

Del Corral, J. M., Miralles, A., Nicolau, M. C., Planas, B., & Rial, R. V. (1990). Stereotaxic atlas for the lizard *Gallotia galloti*. Progress in Neurobiology, 34(3), 185–196.

Desfilis, E., Abellán, A., Sentandreu, V., & Medina, L. M. (2018). Expression of regulatory genes in the embryonic brain of a lizard and implications for understanding pallial organization and evolution. Journal of Comparative Neurology, 526(1), 166–202. http://doi.org/10.1002/cne.24329

Díaz, C., Yanes, C., Trujillo, C. M., & Puelles, L. (2000). Cytoarchitectonic subdivisions in the subtectal midbrain of the lizard *Gallotia galloti*. Journal of Neurocytology, 29(8), 569–593.

ten Donkelaar, H. J. (1998). Reptiles. In *The Central Nervous System of Vertebrates* (pp. 1315–1524). Berlin, Germany: Springer.

ten Donkelaar, H. J., & Bangma, G. C. (1992). The Cerebellum. In *Biology of the Reptilia: Sensorimotor Integration* (pp. 496–586). Chicago, IL: University of Chicago Press.

ten Donkelaar, H. J., Bangma, G. C., Barbas-Henry, H. A., Huizen, R., de, B.-V., & Wolters, J. G. (2012). *The Brain Stem in a Lizard, Varanus exanthematicus*. Berlin, Germany: Springer.

Dorr, A. E., Lerch, J. P., Spring, S., Kabani, N., & Henkelman, R. M. (2008). High resolution three-dimensional brain atlas using an average magnetic resonance image of 40 adult C57Bl/6J mice. NeuroImage, 42(1), 60–69. http://doi.org/10.1016/j.neuroimage.2008.03.037

Díaz, C., &., & Glover, J. C. (2002). Comparative aspects of the hodological organization of the vestibular nuclear complex and related neuron populations. Brain Research Bulletin, 57(3-4), 307–312. http://doi.org/10.1016/S0361-9230(01)00673-6

Friedel, M., van Eede, M. C., Pipitone, J., Chakravarty, M. M., & Lerch, J. P. (2014). Pydpiper: a flexible toolkit for constructing novel registration pipelines. Frontiers in Neuroinformatics, 8, 67. http://doi.org/10.3389/fninf.2014.00067

Gibbons, J. R. H. (1979). The Hind Leg Pushup Display of the *Amphibolurus decresii* Species Complex (Lacertilia: Agamidae). Copeia, 1979(1), 29–40.

Gray, J. E. (1827). XI. A synopsis of the genera of Saurian reptiles, in which some new genera are indicated, and the others reviewed by actual examination. Philosophical Magazine Series 2, 2(7), 54–58. http://doi.org/10.1080/14786442708675620

Greenberg, N. (1982). A forebrain atlas and stereotaxic technique for the lizard, *Anolis carolinensis*. Journal of Morphology, 174(2), 217–236.

Halpern, M. (1980). The telencephalon of snakes. In S. O. E. Ebbesson (Ed.), *Comparative Neurology of the Telencephalon* (pp. 257–295). Boston, MA: Springer US. http://doi.org/10.1007/978-1-4613-2988-6_9

Hamilton, A. J., May, R. M., & Waters, E. K. (2015). Zoology: Here be dragons. Nature, 520, 42–43. http://doi.org/10.1038/520042a

Healey, M. (2008). *The evolution of colour polymorphism in the painted dragon, Ctenophorus pictus*. (M. Olsson, Ed.). Wollongong, Australia: University of Wollongong.

Herrick, C. J. (1910). The morphology of the forebrain in amphibia and reptilia. The. Journal of Comparative Neurology and Psychology, 20(5), 413–547. http://doi.org/10.1002/cne.920200502

Hoops, D. (2015). A perfusion protocol for lizards, including a method for brain removal. Methods X, 2, 165–173. http://doi.org/10.1016/j.mex.2015.03.005

Hoops, D. (2018). The secret caverns of the dragon's brain: Current and potential contributions of lizards to evolutionary neuroscience. Brain, Behavior and Evolution, 1–3. http://doi.org/10.1159/000486529

Hoops, D., Ullmann, J. F. P., Janke, A. L., Vidal-García, M., Stait Gardner, T., Dwihapsari, Y. *et al*. (2017a). Sexual selection predicts brain structure in dragon lizards. Journal of Evolutionary Biology, 30(2), 244–256. http://doi.org/10.1111/jeb.12984

Hoops, D., Vidal-García, M., Ullmann, J. F. P., Janke, A. L., Stait-Gardner, T., Duchêne, D. A. *et al*. (2017b). Evidence for concerted and mosaic brain evolution in dragon lizards. Brain, Behavior and Evolution, 90(3), 211–223. http://doi.org/10.1159/000478738

Hyare, H., Powell, C., Thornton, J. S., Mancini, L., Yousry, T., Brandner, S., & So, P.-W. (2008). Perfluoropolyethers in magnetic resonance microscopy: Effect on quantitative magnetic resonance imaging measures and histological properties of formalin-fixed brain tissue. Proceedings of the International Society for Magnetic Resonance in Medicine, 16, 1719.

Iwaniuk, A. N. (2010). Comparative brain collections are an indispensable resource for evolutionary neurobiology. Brain, Behavior and Evolution, 76(2), 87–88. http://doi.org/10.1159/000320214

Iwaniuk, A. N. (2011). The importance of scientific collecting and natural history museums for comparative neuroanatomy. Annals of the New York Academy of Sciences, 1225(S1), E1–E19. http://doi.org/10.1111/j.1749-6632.2011.05977.x

Janke, A. L., & Ullmann, J. F. P. (2015). Robust methods to create ex vivo minimum deformation atlases for brain mapping. Methods, 73, 18–26. http://doi.org/10.1016/j.ymeth.2015.01.005

Kabli, S., Alia, A., Spaink, H. P., Verbeek, F. J., & De Groot, H. J. M. (2006). Magnetic resonance microscopy of the adult zebrafish. Zebrafish, 3(4), 431–439. http://doi.org/10.1089/zeb.2006.3.431

Kupffer, V. K. (1906). *Die Morphogenie des Centralnervensystems*. Jena, Germany: Hertwigs Handbuch der vergleichenden Entwicklungslehre der Wirbeltiere.

LaDage, L. D., Maged, R. M., Forney, M. V., Roth, T. C., Sinervo, B., & Pravosudov, V. V. (2013). Interaction between territoriality, spatial environment, and hippocampal neurogenesis in male side-blotched lizards. Behavioral Neuroscience, 127(4), 555–565. http://doi.org/10.1037/a0032852

LaDage, L. D., Riggs, B. J., Sinervo, B., & Pravosudov, V. V. (2009). Dorsal cortex volume in male side-blotched lizards (*Uta stansburiana*) is associated with different space use strategies. Animal Behaviour, 78(1), 91–96. http://doi.org/10.1016/j.anbehav.2009.03.020

Lanuza, E., & Halpern, M. (1997). Afferent and efferent connections of the nucleus sphericus in the snake *Thamnophis sirtalis*: Convergence of olfactory and vomeronasal information in the lateral cortex and the amygdala. The Journal of Comparative Neurology, 385(4), 627–640. http://doi.org/10.1002

Leal, M., & Powell, B. J. (2012). Behavioural flexibility and problem-solving in a tropical lizard. Biology Letters, 8(1), 28–30. http://doi.org/10.1098/rsbl.2011.0480

Lerch, J. P., Carroll, J. B., Spring, S., Bertram, L. N., Schwab, C., Hayden, M. R., & Henkelman, R. M. (2008). Automated deformation analysis in the YAC128 Huntington disease mouse model. NeuroImage, 39(1), 32–39. http://doi.org/10.1016/j.neuroimage.2007.08.033

Lohman, A. H. M., & Smeets, W. J. A. J. (1993). Overview of the main and accessory olfactory bulb projections in reptiles. Brain, Behavior and Evolution, 41(3-5), 147–155.

Lutterschmidt, D. I., & Maine, A. R. (2014). Sex or candy? Neuroendocrine regulation of the seasonal transition from courtship to feeding behavior in male red-sided garter snakes (*Thamnophis sirtalis parietalis*). Hormones and Behavior, 66(1), 120–134. http://doi.org/10.1016/j.yhbeh.2014.01.011

Maldjian, J. A., Daunais, J. B., Friedman, D. P., & Whitlow, C. T. (2014). Vervet MRI atlas and label map for fully automated morphometric analyses. Neuroinformatics, 12(4), 543–550. http://doi.org/10.1007/s12021-014-9231-8

Marín, F., & Puelles, L. (1995). Morphological fate of rhombomeres in quail/chick chimeras: A segmental analysis of hindbrain nuclei. European Journal of Neuroscience, 7(8), 1714–1738. http://doi.org/10.1111/j.1460-9568.1995.tb00693.x

Martin, J., & Lopez, P. (2000). Chemoreception, symmetry and mate choice in lizards. Proceedings of the Royal Society of London. Series B: Biological Sciences, 267(1450), 1265–1269. http://doi.org/10.1098/rspb.2000.1137

Martinez-Guijarro, F. J., Desfilis, E., & Lopez-Garcia, C. (1990). Organization of the dorsomedial cortex in the lizard *Podarcis hispanica*. In *The Forebrain in Nonmammals: New Aspects of Structure and Development* (pp. 77–92. Berlin, Germany: Springer-Verlag Berlin.

Martínez, S., Marín, F., Nieto, M. A., & Puelles, L. (1995). Induction of ectopic engrailed expression and fate change in avian rhombomeres: Intersegmental boundaries as barriers. Mechanisms of Development, 51(2–3), 289–303. http://doi.org/10.1016/0925-4773(95)00376-2

Martínez-García, F., Olucha, F. E., Teruel, V., Lorente, M. J., & Schwerdtfeger, W. K. (1991). Afferent and efferent connections of the olfactory bulbs in the lizard *Podarcis hispanica*. The Journal of Comparative Neurology, 305(2), 337–347. http://doi.org/10.1002/cne.903050214

McLean, C. A., & Stuart-Fox, D. M. (2014). Geographic variation in animal colour polymorphisms and its role in speciation. Biological Reviews, 89(4), 860–873. http://doi.org/10.1111/brv.12083

McLean, C. A., Stuart-Fox, D. M., & Moussalli, A. (2014). Phylogeographic structure, demographic history and morph composition in a colour polymorphic lizard. Journal of Evolutionary Biology, 27(10), 2123–2137. http://doi.org/10.1111/jeb.12464

Medina, L. M. (2006). Field homologies. In J. H. Kaas (Ed.), *Evolution of Nervous Systems: A Comprehensive Reference*. San Diego, CA: Elsevier Academic Press.

Medina, L. M., Marti, E., Artero, C., Fasolo, A., & Puelles, L. (1992). Distribution of neuropeptide Y-like immunoreactivity in the brain of the lizard *Gallotia galloti*. Journal of Comparative Neurology, 319, 387–405.

Medina, L. M., Puelles, L., & Smeets, W. J. A. J. (1994). Development of catecholamine systems in the brain of the lizard *Gallotia galloti*. The Journal of Comparative Neurology, http://doi.org/10.1002/cne.903500104

Medina, L. M., Smeets, W. J. A. J., Hoogland, P. V., & Puelles, L. (1993). Distribution of choline acetyltransferase immunoreactivity in the brain of the lizard *Gallotia galloti*. The Journal of Comparative Neurology, http://doi.org/10.1002/cne.903310209

Melville, J., Ritchie, E. G., Chapple, S. N. J., Glor, R. E., & Schulte, J. A., I. I. (2011). Evolutionary origins and diversification of dragon lizards in Australia's tropical savannas. Molecular Phylogenetics and Evolution, 58(2), 257–270. http://doi.org/10.1016/j.ympev.2010.11.025

Nieuwenhuys, R., & Puelles, L. (2015). The (Complex) Rostral Part of the Brain. In *Towards a New Neuromorphology* (pp. 125–130). Cham, Switzerland: Springer.

Nieuwenhuys, R., ten Donkelaar, H. J., & Nicholson, C. (1998). *The Central Nervous System of Vertebrates*. Berlin, Germany: Springer.

Northcutt, R. G. (1967). Architectonic studies of the telencephalon of *Iguana iguana*. The Journal of Comparative Neurology, 130(2), 109–147. http://doi.org/10.1002/cne.901300203

Northcutt, R. G. (2013). Variation in reptilian brains and cognition. Brain, Behavior and Evolution, 82(1), 45–54. http://doi.org/10.1159/000351996

Olsson, M., Schwartz, T., Uller, T., & Healey, M. (2009). Effects of sperm storage and male colour on probability of paternity in a polychromatic lizard. Animal Behaviour, 77(2), 419–424. http://doi.org/10.1016/j.anbehav.2008.10.017

Orr, H. (1896). Contribution to the embryology of the lizard. In *Contributions from the biological laboratories in Princeton University*. Princeton, NJ: The Princeton Press.

Osborne, L. (2005a). Information content of male agonistic displays in the territorial tawny dragon (*Ctenophorus decresii*). Journal of Ethology, 23(2), 189–197. http://doi.org/10.1007/s10164-005-0151-9

Osborne, L. (2005b). Rival recognition in the territorial tawny dragon (*Ctenophorus decresii*). Acta Ethologica, 8(1), 45–50. http://doi.org/10.1007/s10211-005-0108-6

Osborne, L., Umbers, K. D. L., & Keogh, J. S. (2013). The effects of perch height, time in residence and distance from opponent on aggressive display in male lizards. Acta Ethologica, http://doi.org/10.1007/s10211-012-0135-z

Osborne, L., Umbers, K. D. L., Backwell, P. R. Y., & Keogh, J. S. (2012). Male tawny dragons use throat patterns to recognize rivals. Naturwissenschaften, 99(10), 869–872. http://doi.org/10.1007/s00114-012-0968-3

Paxinos, G., & Franklin, K. B. J. (2013). *Paxinos and Franklin's The Mouse Brain in Stereotaxic Coordinates* (4 ed.). San Diego, CA: Elsevier Academic Press.

Paxinos, G., & Watson, C. (2013). *Paxinos and Watson's The Rat Brain in Stereotaxic Coordinates* (7 ed.). San Diego, CA: Elsevier Academic Press.

Peterson, E. H. (1981). Patterns of olfactory projections in the desert iguana, *Dipsosaurus dorsalis*. Journal of Morphology, 168(2), 189–227.

Platel, M. R. (1976). Analyse volumétrique comparée des principales subdivisions encéphaliques chez les reptiles sauriens. Journal Für Hirnforschung, 17, 513–537.

Poirier, C., Vellema, M., Verhoye, M., Van Meir, V., Wild, J. M., Balthazart, J., & Van der Linden, A. (2008). A three-dimensional MRI atlas of the zebra finch brain in stereotaxic coordinates. NeuroImage, 41(1), 1–6. http://doi.org/10.1016/j.neuroimage.2008.01.069

Powell, B. J., & Leal, M. (2014). Brain organization and habitat complexity in *Anolis* lizards. Brain, Behavior and Evolution, 84(1), 8–18. http://doi.org/10.1159/000362197

Powers, A., & Reiner, A. (1980). A stereotaxic atlas of the forebrain and midbrain of the eastern painted turtle (*Chrysemys picta picta*). Journal Fur Hirnforschung, 21(2), 125–159.

Puelles, L. (2009). Forebrain development: Prosomere model. In L. R. Squire (Ed.), *Encyclopedia of Neuroscience* (Vol. 4, pp. 315–319. San Diego, CA: Elsevier Academic Press.

Puelles, L., & Medina, L. M. (2002). Field homology as a way to reconcile genetic and developmental variability with adult homology. Brain Research Bulletin, 57(3-4), 243–255.

Puelles, L., & Rubenstein, J. L. R. (1993). Expression patterns of homeobox and other putative regulatory genes in the embryonic mouse forebrain suggest a neuromeric organization. Trends in Neurosciences, 16(11), 472–479. http://doi.org/10.1016/0166-2236(93)90080-6

Puelles, L., & Rubenstein, J. L. R. (2003). Forebrain gene expression domains and the evolving prosomeric model. Trends in Neurosciences, 26(9), 469–476. http://doi.org/10.1016/S0166-2236(03)00234-0

Puelles, L., & Rubenstein, J. L. R. (2015). A new scenario of hypothalamic organization: rationale of new hypotheses introduced in the updated prosomeric model. Frontiers in Neuroanatomy, 9, 162–1229. http://doi.org/10.3389/fnana.2015.00027

Puelles, L., Harrison, M., Paxinos, G., & Watson, C. (2013). A developmental ontology for the mammalian brain based on the prosomeric model. Trends in Neurosciences, 36(10), 570–578. http://doi.org/10.1016/j.tins.2013.06.004

Puelles, L., Martínez-de-la-Torre, M., Paxinos, G., Watson, C., & Martinez, S. (2007). *The Chick Brain in Stereotaxic Coordinates: An Atlas Featuring Neuromeric Subdivisions and Mammalian Homologies*. San Diego, CA: Elsevier Academic Press.

Puelles, L., Sandoval, J. E., Ayad, A., D., Corral, R., Alonso, A., Ferran, J. L., & Martínez-de-la-Torre, M. (2006). The Pallium in Reptiles and Birds in the Light of the Updated Tetrapartite Pallium Model. In J. H. Kaas (Ed.), *Evolution of Nervous Systems: A Comprehensive Reference* (2ne ed., Vol. 1, pp. 519–555). San Diego, CA: Elsevier Academic Press. http://doi.org/10.1016/B978-0-12-804042-3.00014-2

Pyron, R. A., Burbrink, F. T., & Wiens, J. J. (2013). A phylogeny and revised classification of Squamata, including 4161 species of lizards and snakes. BMC Evolutionary Biology, 13(1), 93. http://doi.org/10.1186/1471-2148-13-93

Ramón y Cajal, S. (1891). Sur la fine structure du lobe optique des oiseaux et sur l'origine réelle des nerfs optiques. International Monatsschrift in Anatomy and Physiology, 8, 337–366.

Reeder, T. W., Townsend, T. M., Mulcahy, D. G., Noonan, B. P., Wood, P. L., Jr, Sites, J. W., Jr., & Wiens, J. J. (2015). Integrated analyses resolve conflicts over squamate reptile phylogeny and reveal unexpected placements for fossil taxa. PLoS One, 10(3), e0118199. http://doi.org/10.1371/journal.pone.0118199

Robinson, C. D., Patton, M. S., Andre, B. M., & Johnson, M. A. (2015). Convergent evolution of brain morphology and communication modalities in lizards. Current Zoology, 61(2), 281–291. http://doi.org/10.1093/czoolo/61.2.281

Schwab, M. E. (1979). Variation in the rhombencephalon. In C. Gans (Ed.), *Biology of the reptilia: Neurology B* (pp. 201–242). San Diego, CA: Elsevier Academic Press.

Schwenk, K. (1993). The evolution of chemoreception in squamate reptiles: a phylogenetic approach. Brain, Behavior and Evolution, 41(3-5), 124–137.

Shimamura, K., Hartigan, D. J., Martínez, S., Puelles, L., & Rubenstein, J. L. (1995). Longitudinal organization of the anterior neural plate and neural tube. Development (*Cambridge*, England), 121(12), 3923–3933.

Simões, J. M., Teles, M. C., Oliveira, R. F., Van der Linden, A., & Verhoye, M. (2012). A three-dimensional stereotaxic MRI brain atlas of the cichlid fish *Oreochromis mossambicus*. PLoS One, 7(9), e44086. http://doi.org/10.1371/journal.pone.0044086

Sled, J. G., Zijdenbos, A. P., & Evans, A. C. (1998). A nonparametric method for automatic correction of intensity nonuniformity in MRI data. IEEE Transactions on Medical Imaging, 17(1), 87–97. http://doi.org/10.1109/42.668698

Smeets, W. J. A. J., Hoogland, P. V., & Lohman, A. H. M. (1986). A forebrain atlas of the lizard *Gekko gecko*. The Journal of Comparative Neurology, 254(1), 1–19. http://doi.org/10.1002/cne.902540102

Striedter, G. F. (2005). *Principles of Brain Evolution*. Sunderland, MA: Sinauer Associates.

Stuart-Fox, D. M., & Owens, I. P. F. (2003). Species richness in agamid lizards: chance, body size, sexual selection or ecology?. Journal of Evolutionary Biology, 16(4), 659–669.

Stuart-Fox, D. M., Moussalli, A., Johnston, G. R., & Owens, I. P. F. (2004). Evolution of color variation in dragon lizards: Quantitative tests of the role of crypsis and local adaptation. Evolution, 58(7), 1549–1559. http://doi.org/10.1554/03-448

Teasdale, L. C., Stevens, M., & Stuart-Fox, D. M. (2013). Discrete colour polymorphism in the tawny dragon lizard (*Ctenophorus decresii*) and differences in signal conspicuousness among morphs. Journal of Evolutionary Biology, 26(5), 1035–1046. http://doi.org/10.1111/jeb.12115

Tobler, M., Healey, M., & Olsson, M. (2011). Digit ratio, color polymorphism and egg testosterone in the Australian painted dragon. PLoS One, 6(1), e16225. http://doi.org/10.1371/journal.pone.0016225.t002

Uetz, P., & Hošek, J. (2017). The reptile database. Retrieved from reptile-database.org

Ullmann, J. F. P., Cowin, G., & Collin, S. P. (2010a). Magnetic resonance microscopy of the barramundi (*Lates calcarifer*) brain. Journal of Morphology, 271(12), 1446–1456. http://doi.org/10.1002/jmor.10887

Ullmann, J. F. P., Cowin, G., Kurniawan, N. D., & Collin, S. P. (2010b). A three-dimensional digital atlas of the zebrafish brain. NeuroImage, 51(1), 76–82. http://doi.org/10.1016/j.neuroimage.2010.01.086

Ullmann, J. F. P., Keller, M. D., Watson, C., Janke, A. L., Kurniawan, N. D., Yang, Z. *et al*. (2012). Segmentation of the C57BL/6J mouse cerebellum in magnetic resonance images. NeuroImage, 62(3), 1408–1414. http://doi.org/10.1016/j.neuroimage.2012.05.061

Ullmann, J. F. P., Watson, C., Janke, A. L., Kurniawan, N. D., & Reutens, D. C. (2013a). A segmentation protocol and MRI atlas of the C57BL/6J mouse neocortex. NeuroImage, 78(C), 196–203. http://doi.org/10.1016/j.neuroimage.2013.04.008

Ullmann, J. F. P., Watson, C., Janke, A. L., Kurniawan, N. D., Paxinos, G., & Reutens, D. C. (An MRI atlas of the mouse basal ganglia. Brain Structure and Function, 219(4), 1343–1353. 2013b). http://doi.org/10.1007/s00429-013-0572-0

Umbers, K. D. L., Osborne, L., & Keogh, J. S. (2012). The effects of residency and body size on contest initiation and outcome in the territorial dragon, *Ctenophorus decresii*. PLoS One, 7(10), e47143. http://doi.org/10.1371/journal.pone.0047143

Vellema, M., Verschueren, J., Van Meir, V., & Van der Linden, A. (2011). A customizable 3-dimensional digital atlas of the canary brain in multiple modalities. NeuroImage, 57(2), 352–361. http://doi.org/10.1016/j.neuroimage.2011.04.033

Vercken, E., Massot, M., Sinervo, B., & Clobert, J. (2007). Colour variation and alternative reproductive strategies in females of the common lizard *Lacerta vivipara*. Journal of Evolutionary Biology, 20(1), 221–232. http://doi.org/10.1111/j.1420-9101.2006.01208.x

Vincent, R. D., Neelin, P., Khalili-Mahani, N., Janke, A. L., Fonov, V. S., Robbins, S. M. *et al*. (2016). MINC 2.0: A flexible format for multi-modal images. Frontiers in Neuroinformatics, 10(7), 35. http://doi.org/10.3389/fninf.2016.00035

Watson, C., Janke, A. L., Hamalainen, C., Bagheri, S. M., Paxinos, G., Reutens, D. C., & Ullmann, J. F. P. (2017). An ontologically consistent MRI-based atlas of the mouse diencephalon. NeuroImage, 157, 275–287. http://doi.org/10.1016/j.neuroimage.2017.05.057

Wellenreuther, M., Svensson, E. I., & Hansson, B. (2014). Sexual selection and genetic colour polymorphisms in animals. Molecular Ecology, 23(22), 5398–5414. http://doi.org/10.1111/mec.12935

Whiting, M. J., & While, G. M. (2017). Sociality in Lizards. In D. R. Rubenstein & P. Abbot (Eds.), *Comparative Social Evolution* (pp. 390–426). Cambridge, UK: Cambridge University Press. http://doi.org/10.1017/9781107338319

Wolters, J. G., ten Donkelaar, H. J., & Verhofstad, A. A. (1984). Distribution of catecholamines in the brain stem and spinal cord of the lizard *Varanus exanthematicus*: An immunohistochemical study based on the use of antibodies to tyrosine hydroxylase. Neuroscience, 13(2), 469–493. http://doi.org/10.1016/0306-4522(84)90243-4

Wolters, J. G., ten Donkelaar, H. J., Steinbusch, H., & Verhofstad, A. (1985). Distribution of serotonin in the brain-stem and spinal cord of the lizard *Varanus exanthematicus*: An immunohistochemical study.

Neuroscience, 14(1), 169–193. http://doi.org/10.1016/0306-4522(85)90172-1

Wouterlood, F. G. (1981). The structure of the mediodorsal cerebral cortex in the lizard *Agama agama*: A Golgi study. The Journal of Comparative Neurology, 196(3), 443–458. http://doi.org/10.1002/cne.901960308

Yewers, M. S. C., McLean, C. A., Moussalli, A., Stuart-Fox, D. M., Bennett, A. T. D., & Knott, B. (2015). Spectral sensitivity of cone photoreceptors and opsin expression in two colour-divergent lineages of the lizard *Ctenophorus decresii*. Journal of Experimental Biology, 218(Pt 10), 1556–1563. http://doi.org/10.1242/jeb.119404

Yewers, M. S. C., Pryke, S., & Stuart-Fox, D. M. (2016). Behavioural differences across contexts may indicate morph-specific strategies in the lizard *Ctenophorus decresii*. Animal Behaviour, 111(C), 329–339. http://doi.org/10.1016/j.anbehav.2015.10.029

Yopak, K. E., & Frank, L. R. (2009). Brain size and brain organization of the whale shark, *Rhincodon typus*, using magnetic resonance imaging. Brain, Behavior and Evolution, 74(2), 121–142. http://doi.org/10.1159/000235962

Zamundio, K. R., & Sinervo, B. (2003). Ecological and social contexts for the evolution of alternative mating strategies. In S. F. Fox, T. A. Baird, & J. K. McCoy (Eds.), *Territoriality, Dominance, and Sexual Selection*. Baltimore, MD: Johns Hopkins University Press.

How to cite this article: Hoops D, Desfilis E, Ullmann JFP, et al. A 3D MRI-based atlas of a lizard brain. *J Comp Neurol*. 2018;526:2511–2547. https://doi.org/10.1002/cne.24480

FIGURES 4–20 Coronal sections through the MRI model of the tawny dragon (*Ctenophorus decresii*) brain. Figures are in rostro-caudal order and each section is 25 voxels or 500 μm caudal to the previous section except for Figure 5, which is 250 μm caudal to Figure 4 and 250 μm anterior to Figure 6. The plane of each section according to our coordinate system is indicated in the upper left corner. The bar in the lower right corner = 1 mm. A list of abbreviations is found in Table 1

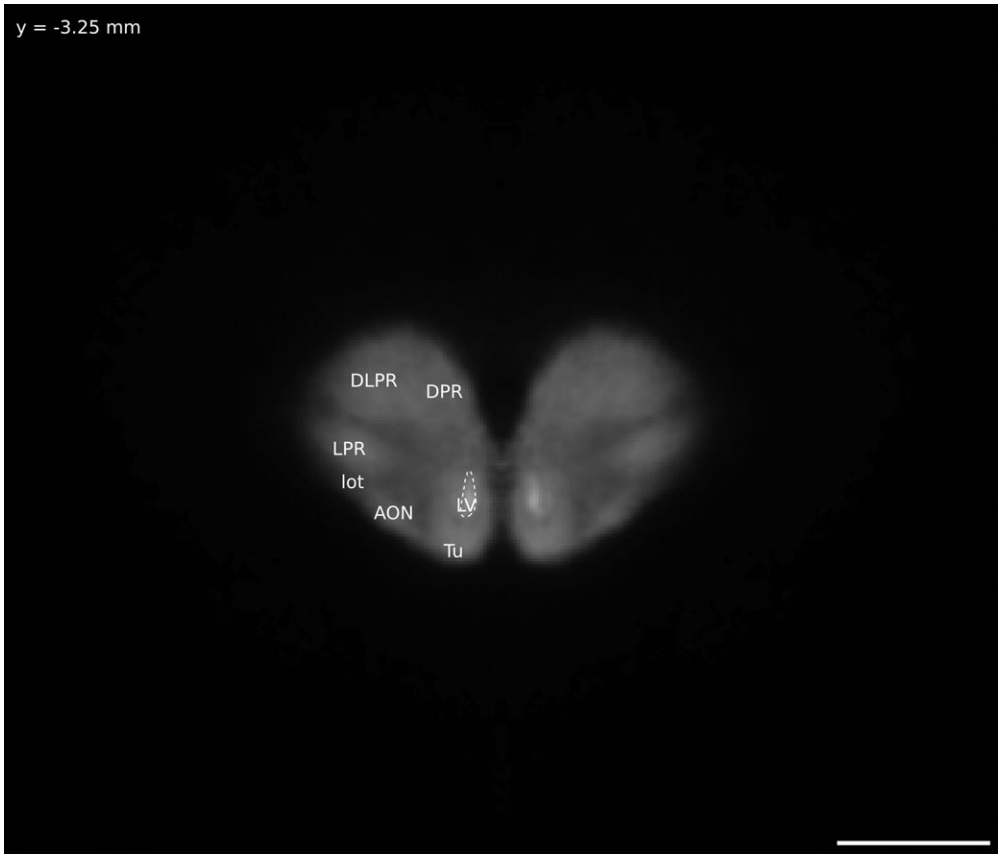

FIGURE 4

FIGURE 5

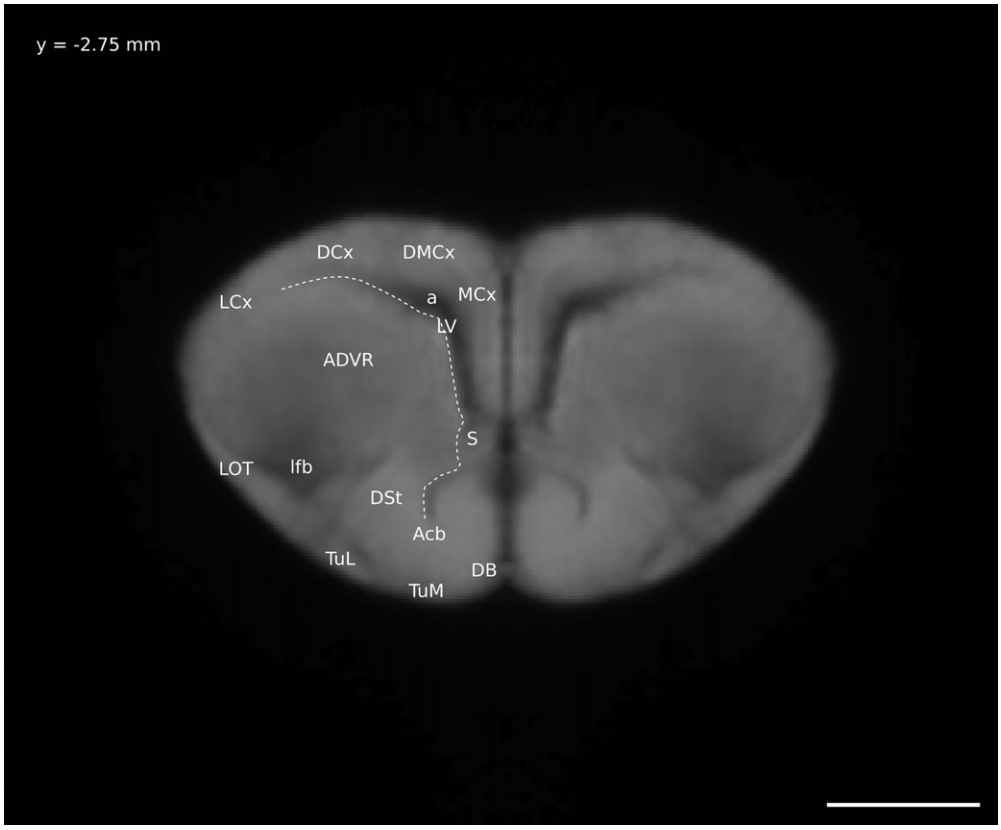

FIGURE 6

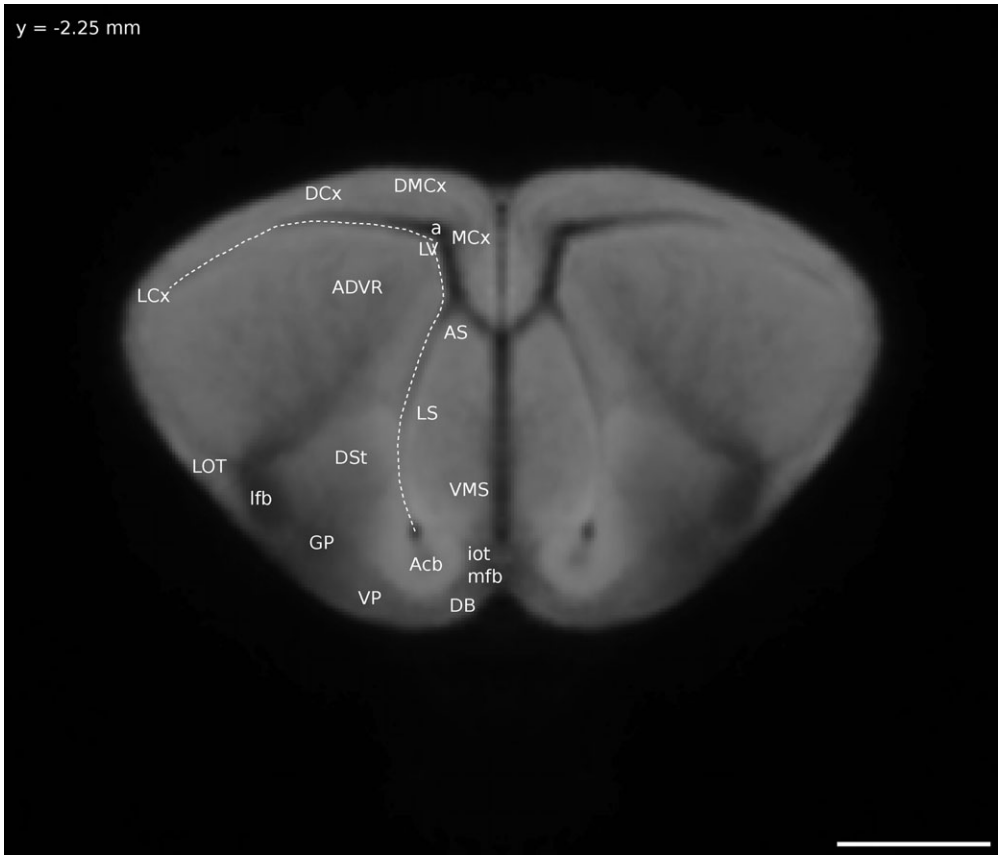

FIGURE 7

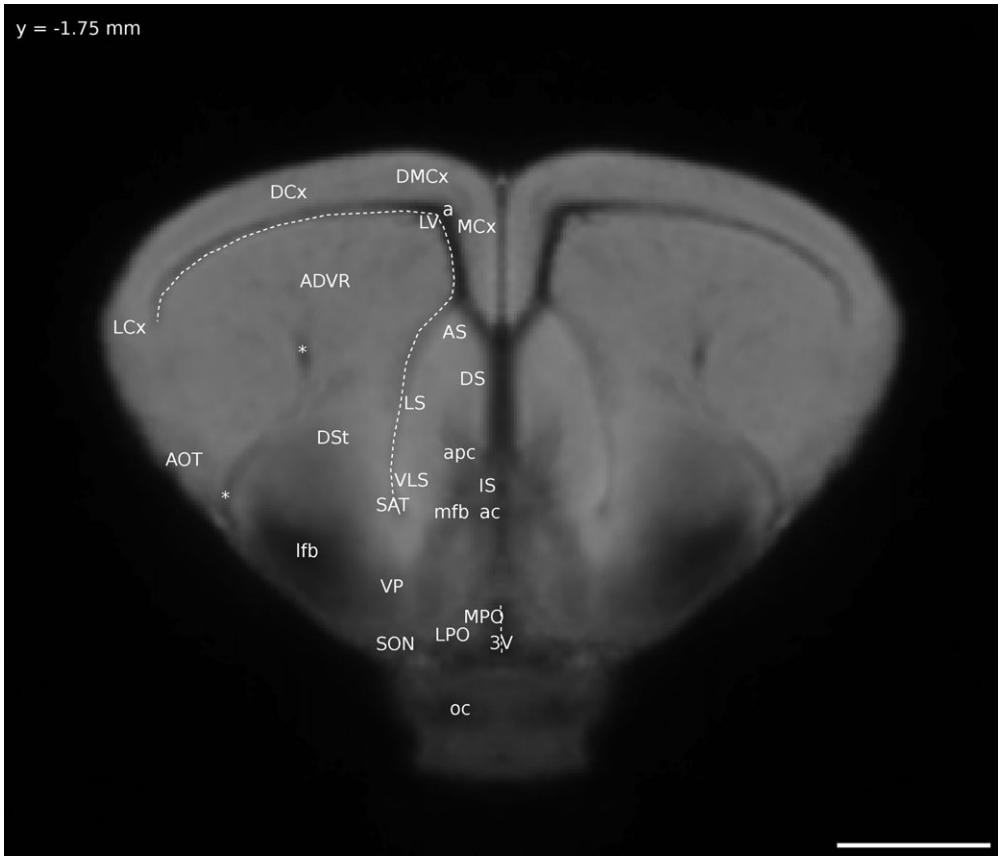

FIGURE 8

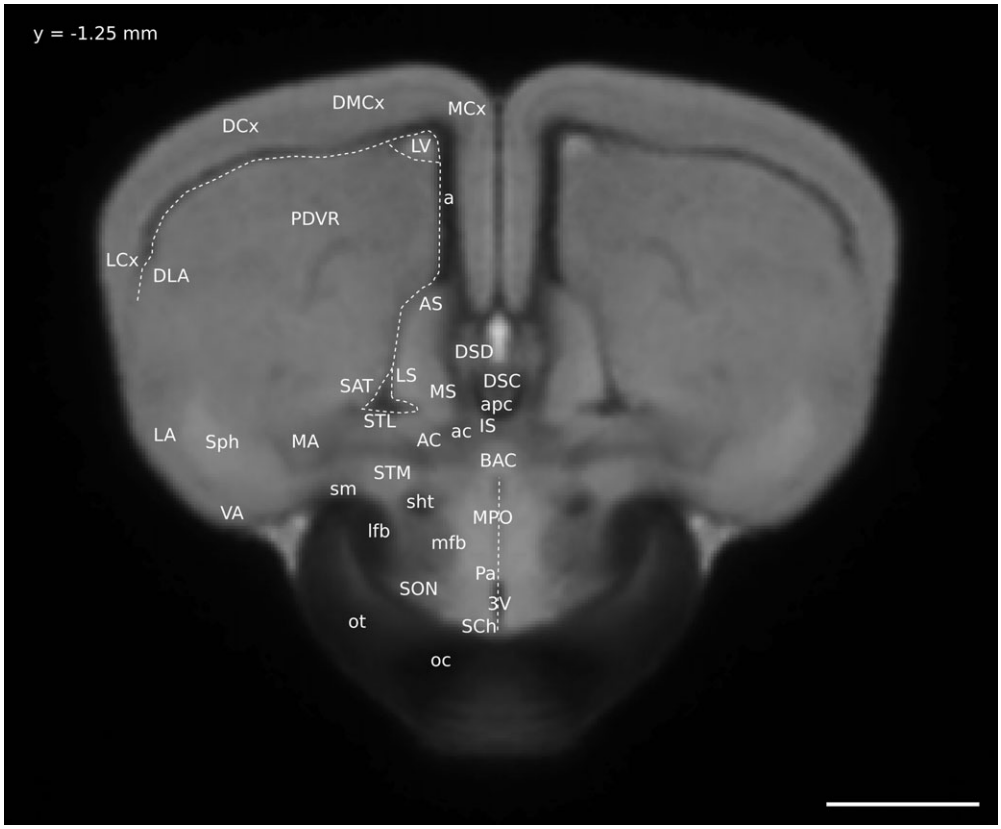

FIGURE 9

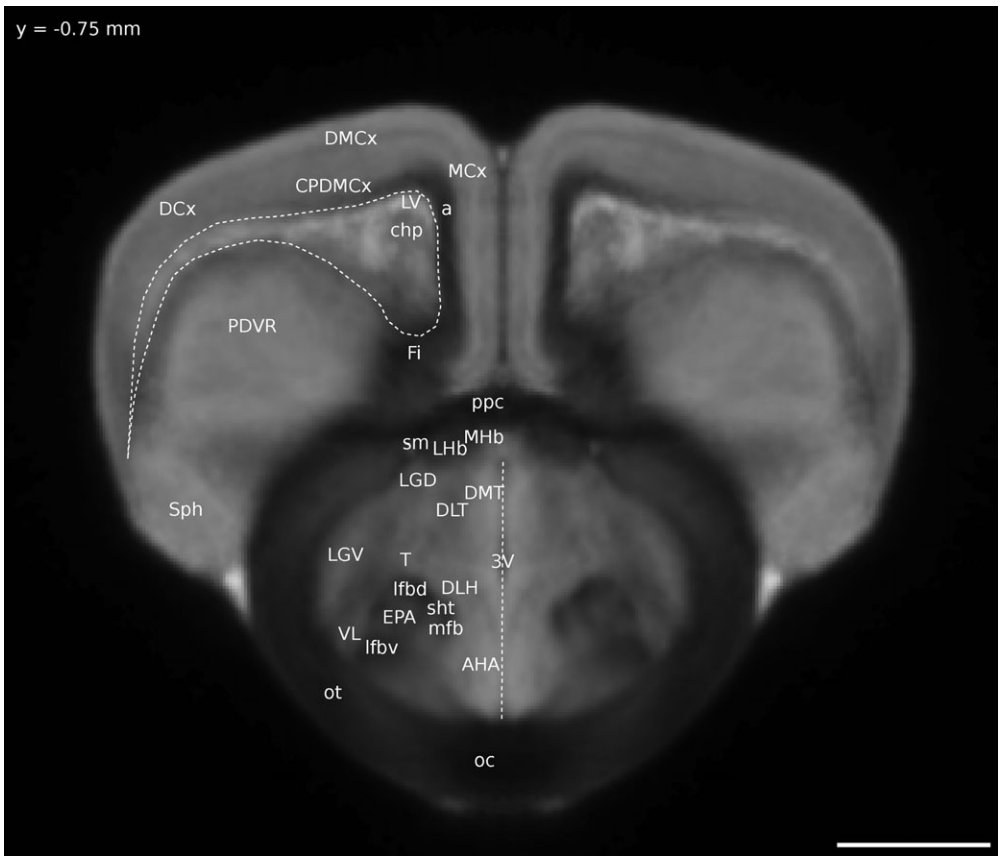

FIGURE 10

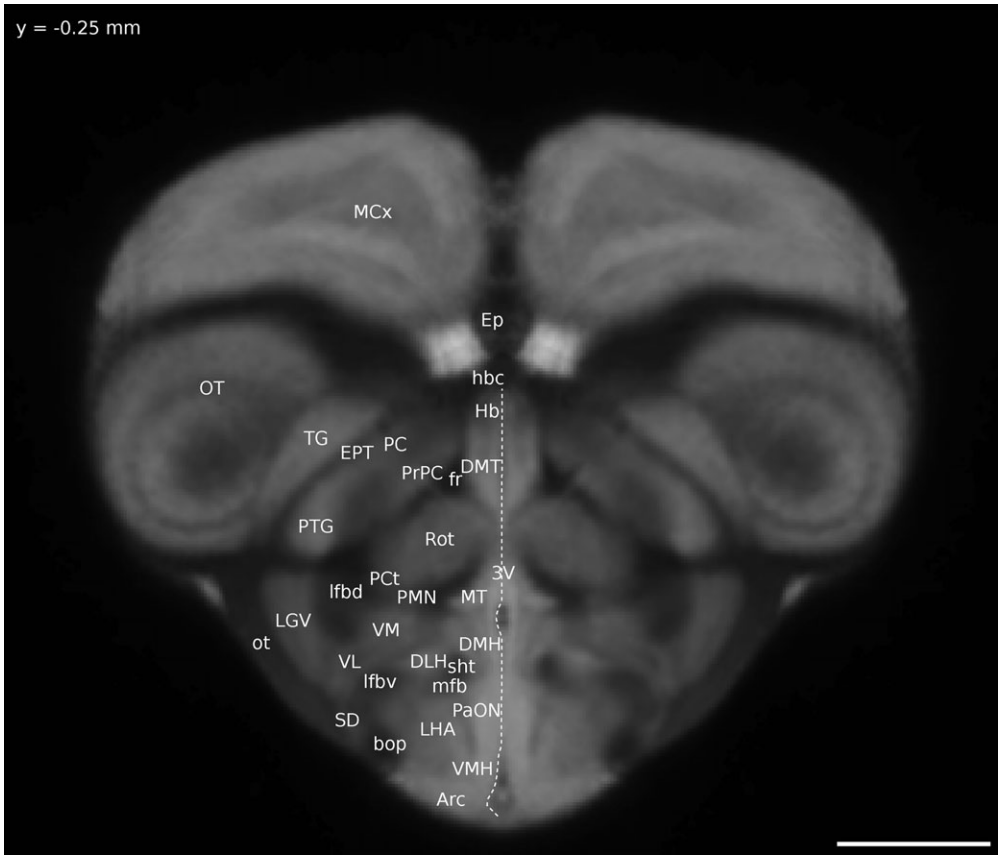

FIGURE 11

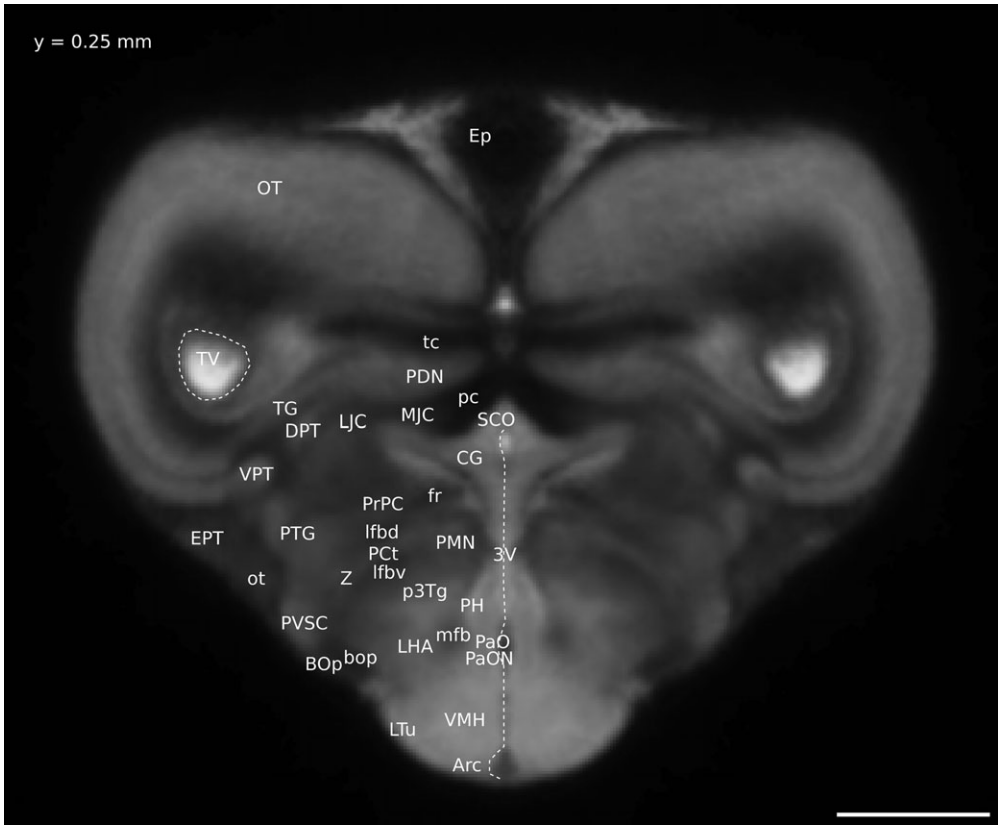

FIGURE 12

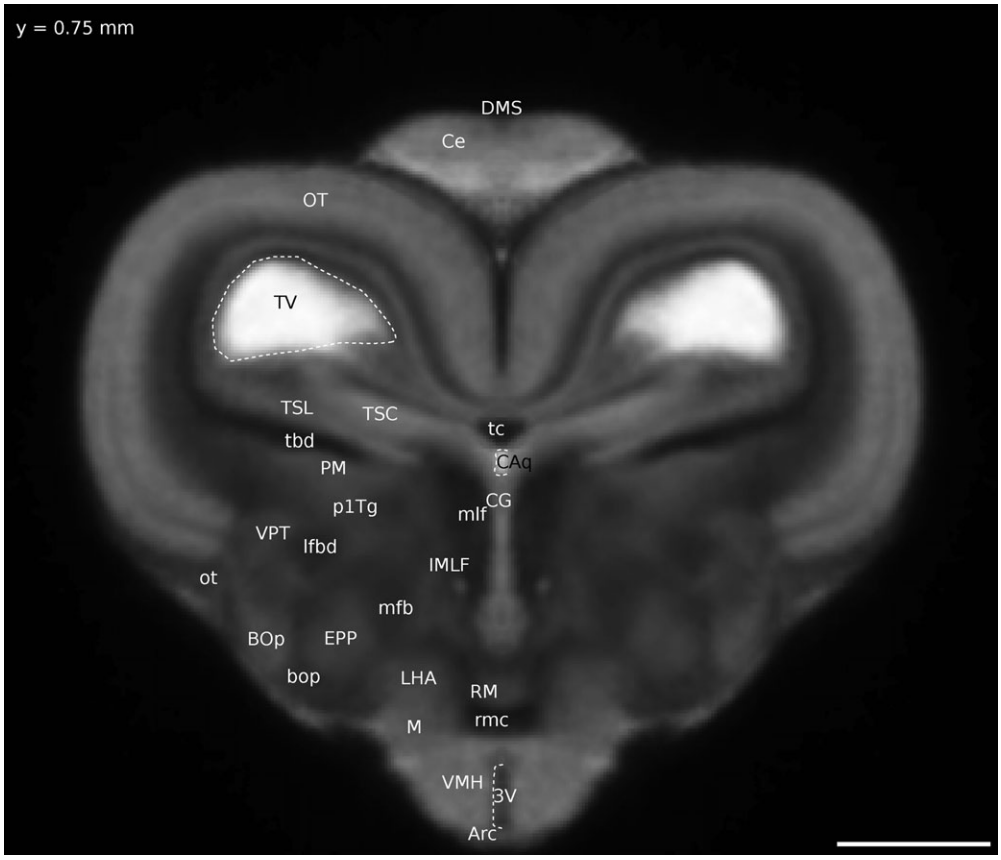

FIGURE 13

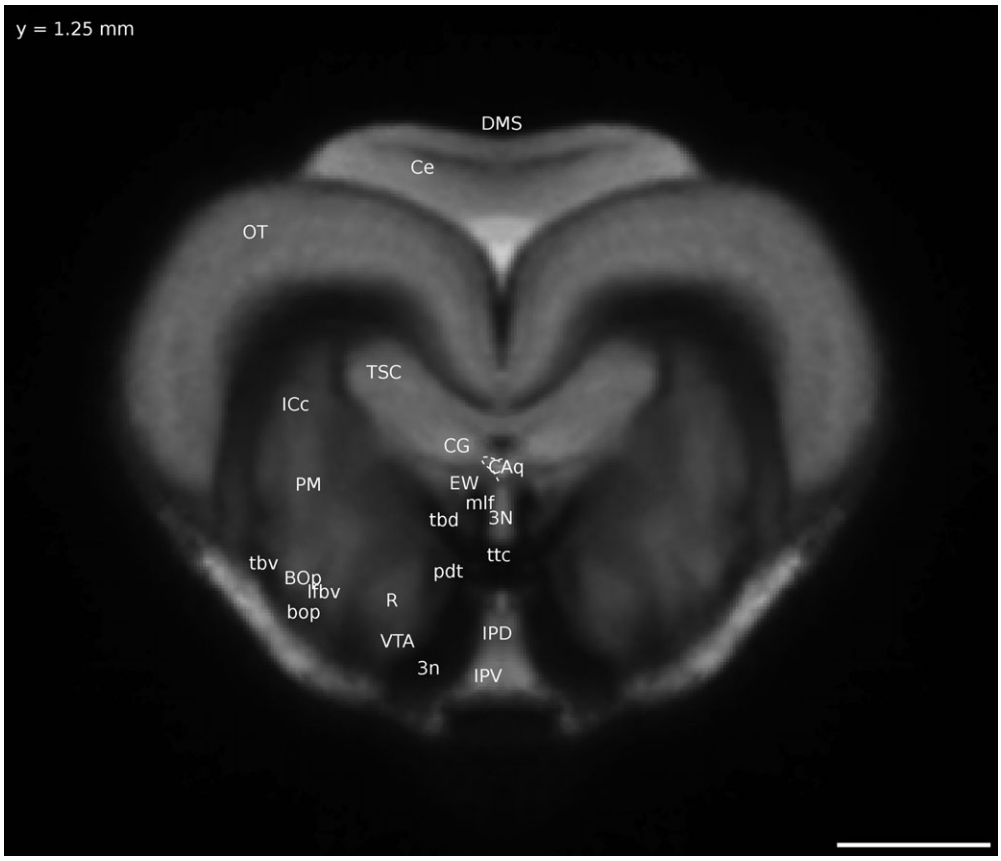

FIGURE 14

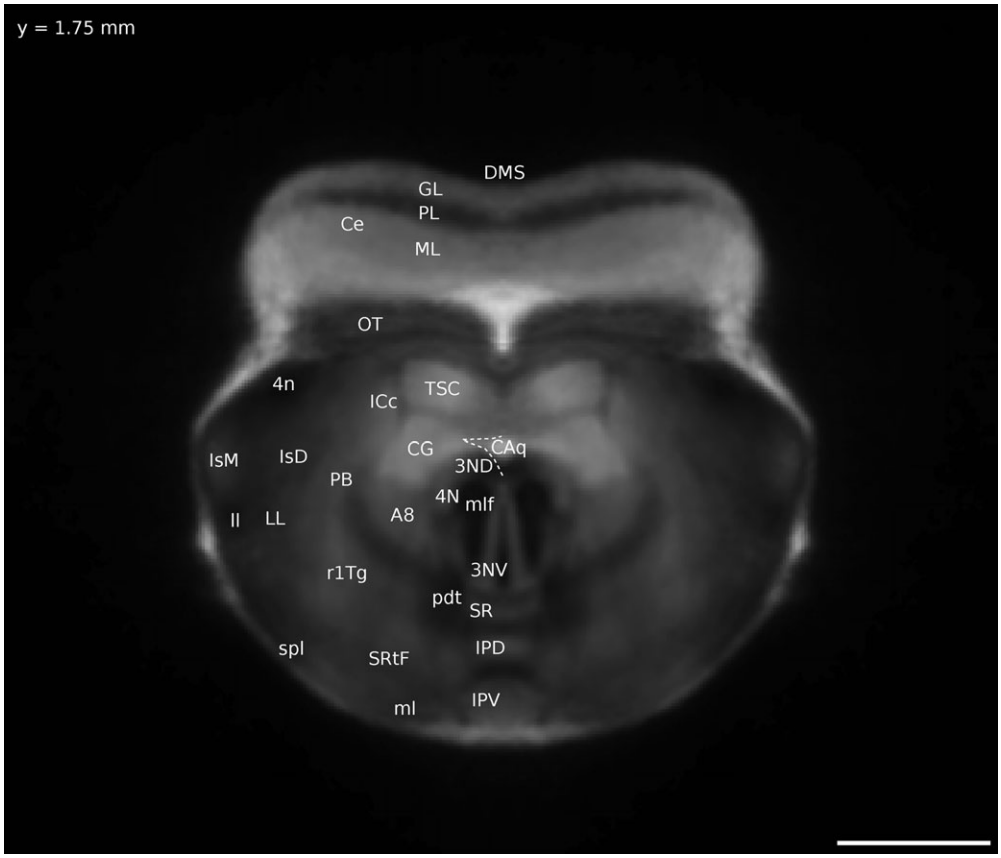

FIGURE 15

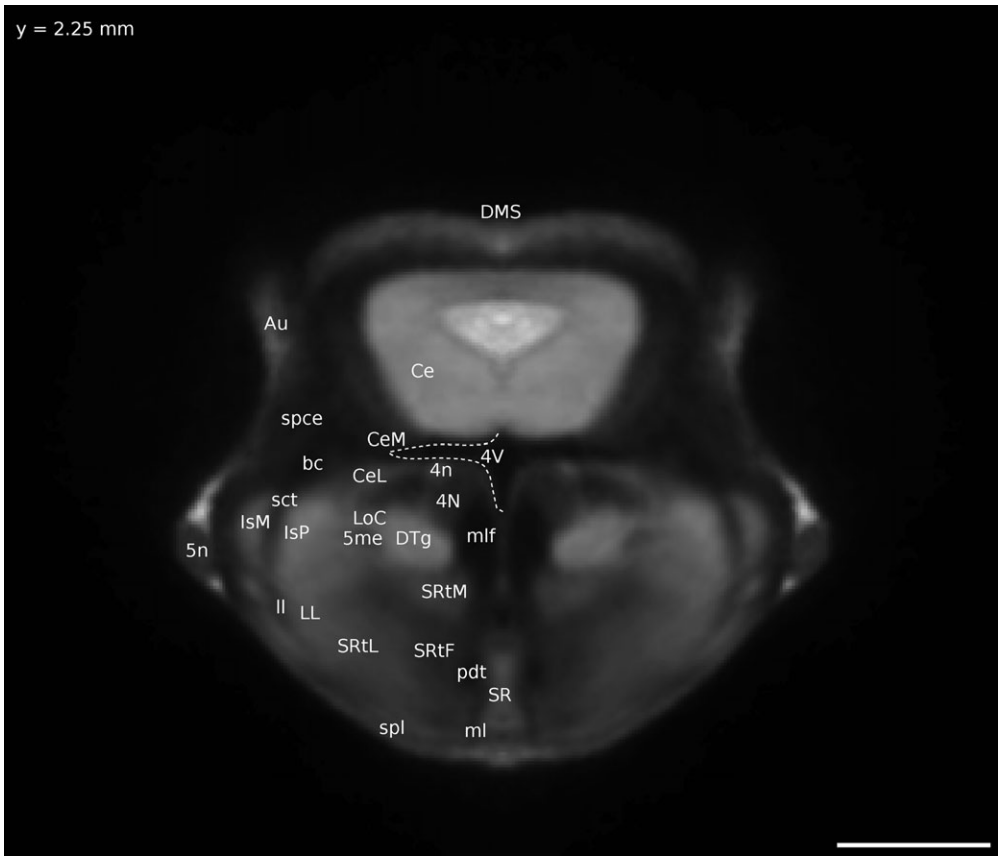

FIGURE 16

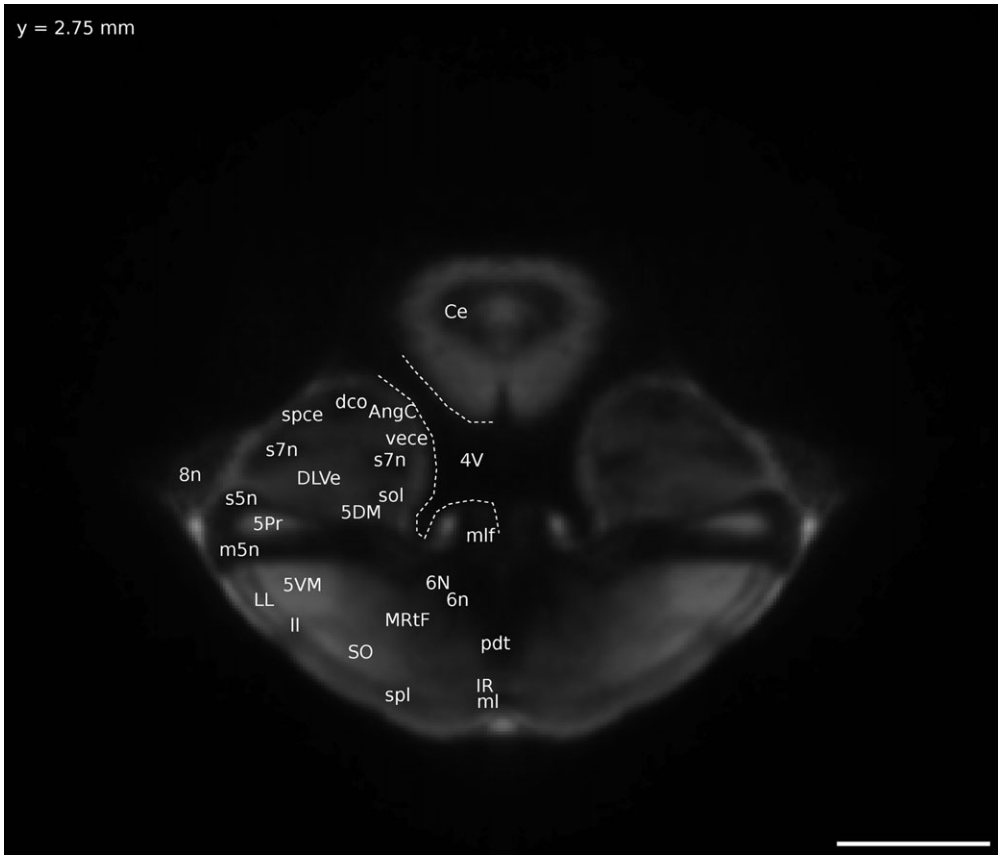

FIGURE 17

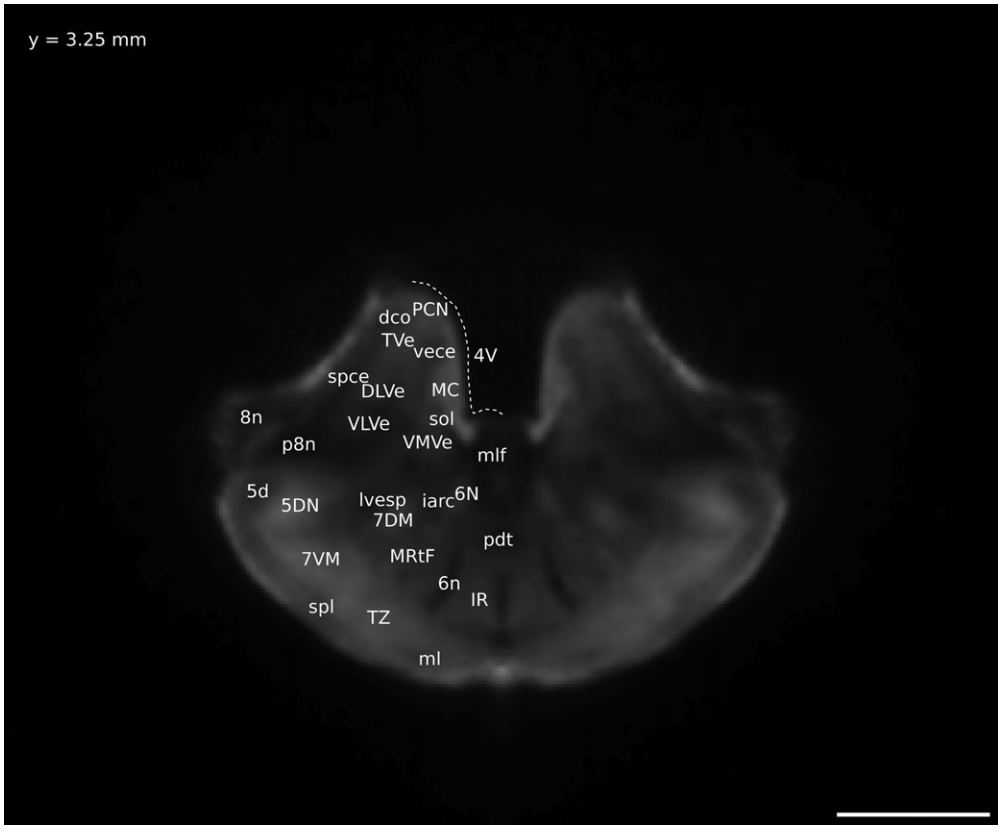

FIGURE 18

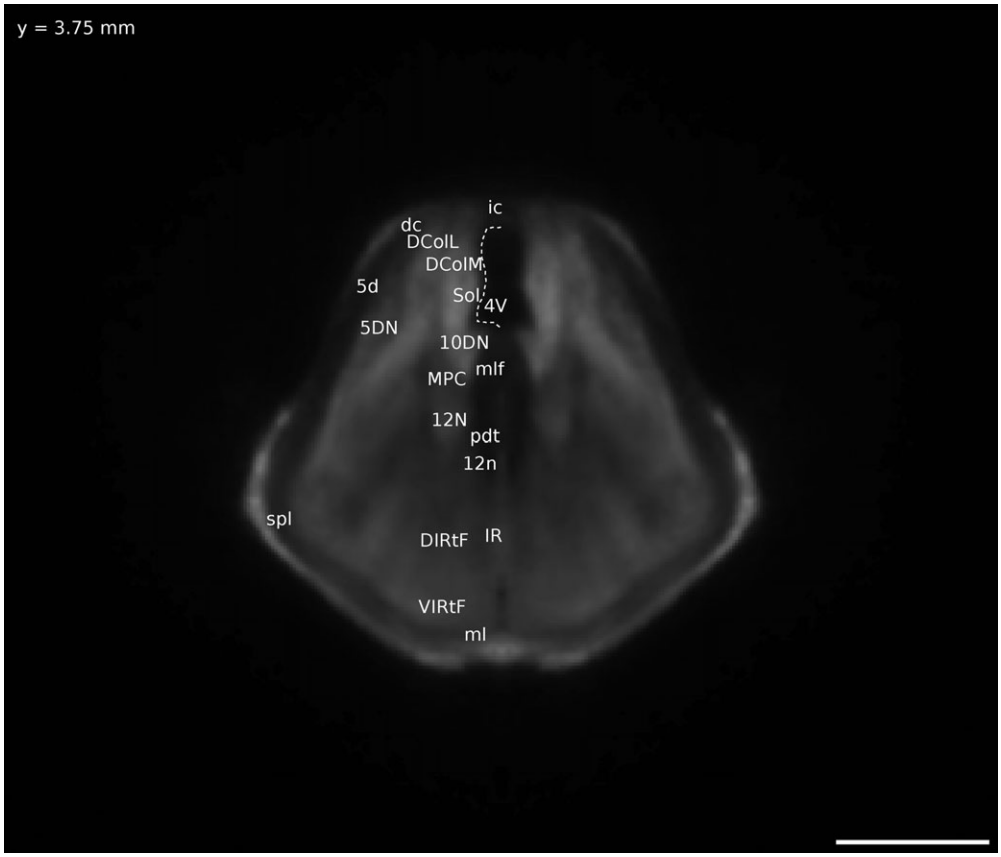

FIGURE 19

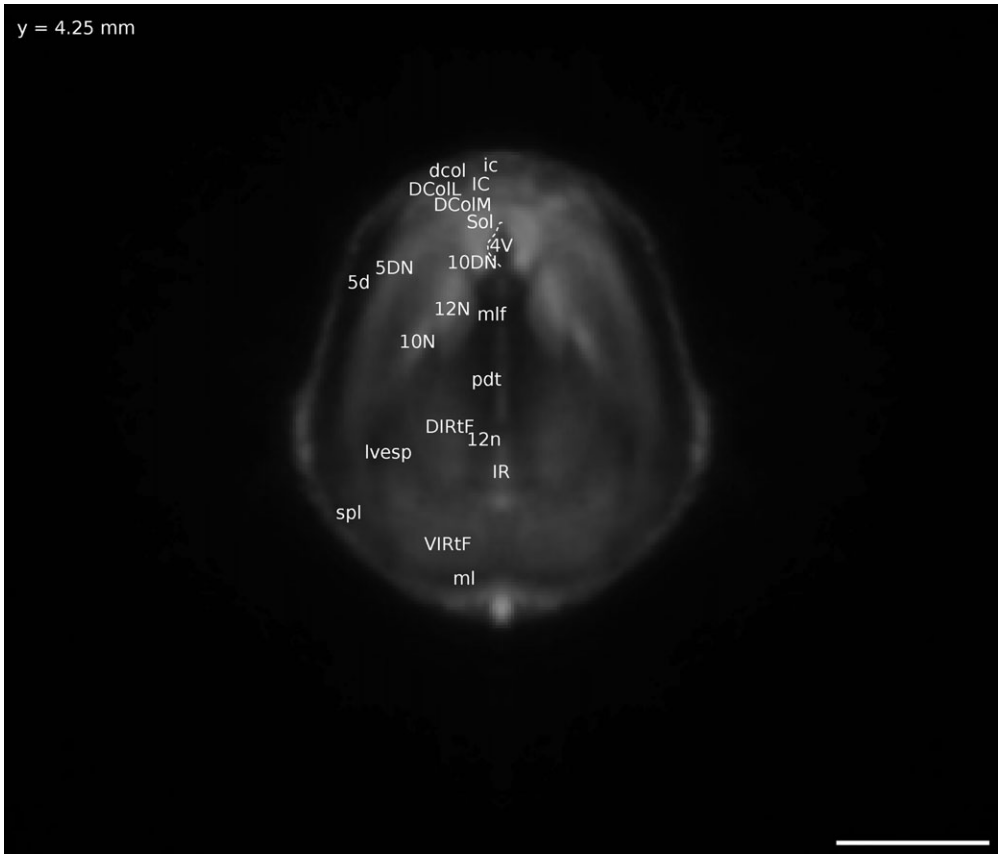

FIGURE 20

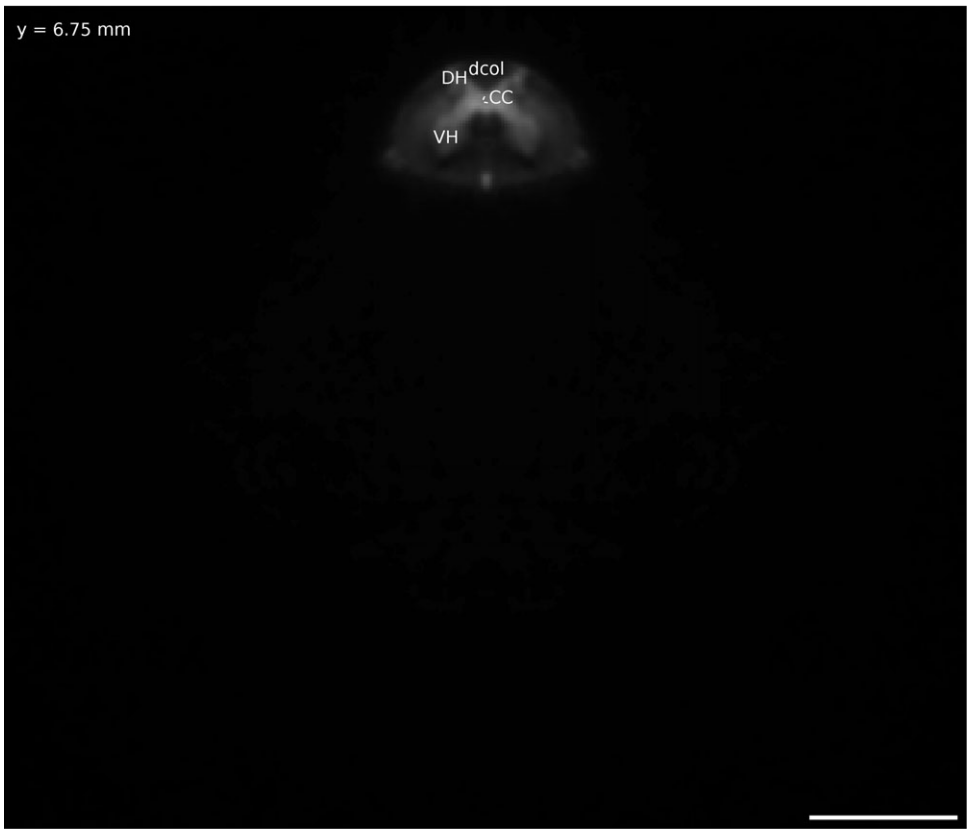

FIGURE 21 A coronal section through the MRI model of the anterior spinal cord of the tawny dragon (*Ctenophorus decresii*). The plane, according to our coordinate system, is indicated in the upper left corner. The bar in the lower right corner = 1 mm. cc = central canal, dc = dorsal column tract, DH = dorsal horn, VH = ventral horn

FIGURES 22–30 Horizontal sections through the MRI model of the tawny dragon (*Ctenophorus decresii*) brain. Figures are in ventro-dorsal order and each section is 25 voxels or 500 μm dorsal to the previous section. The plane of each section according to our coordinate system is indicated in the upper left corner. The bar in the lower right corner = 1 mm. A list of abbreviations is found in Table 1

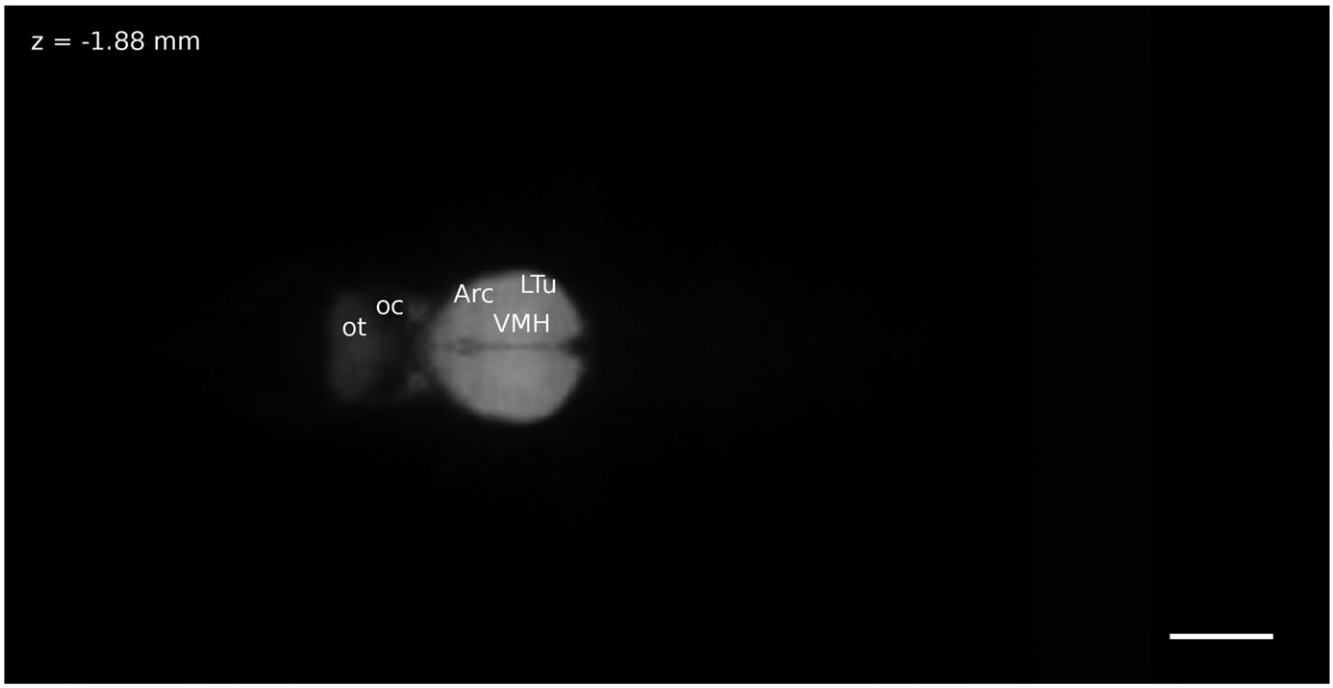

FIGURE 22

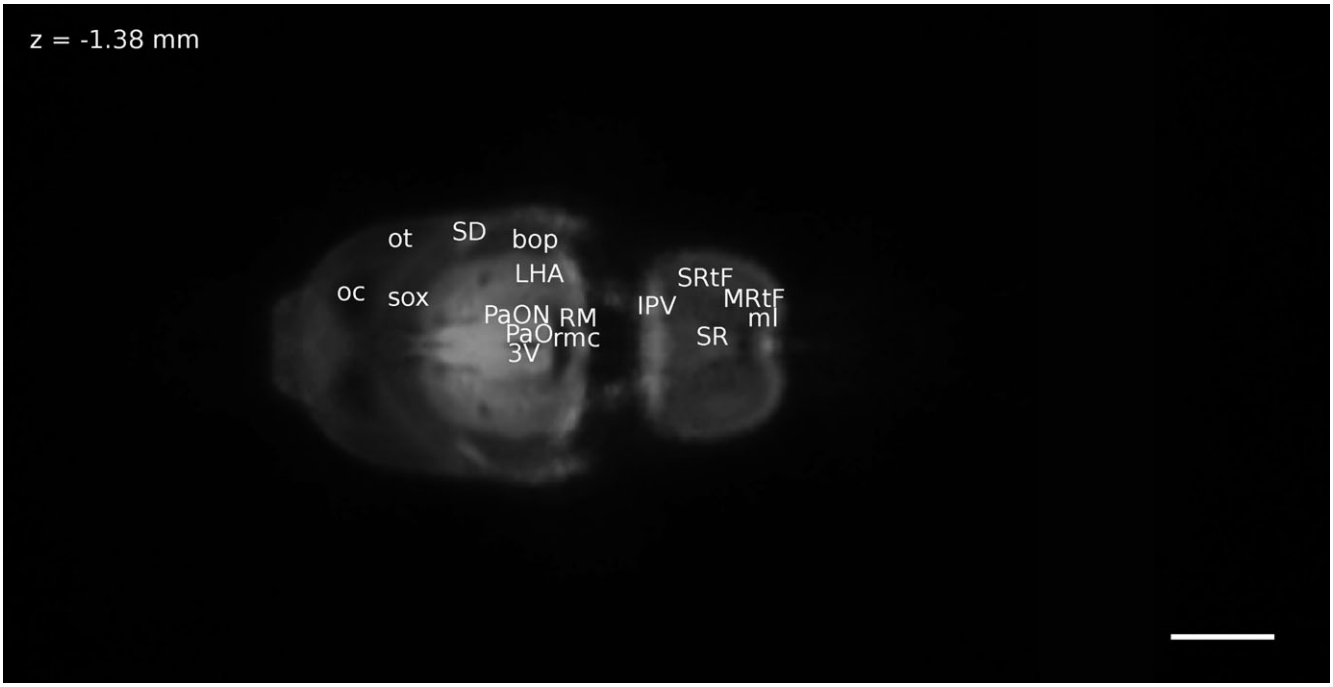

FIGURE 23

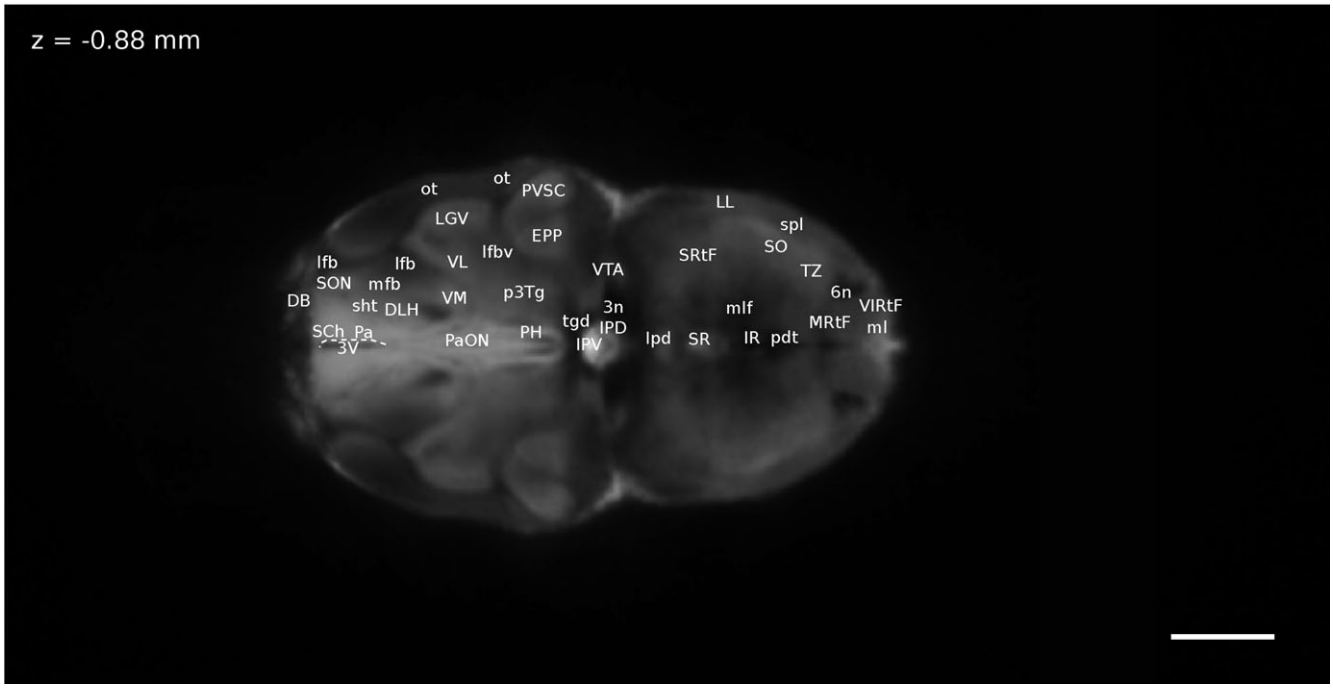

FIGURE 24

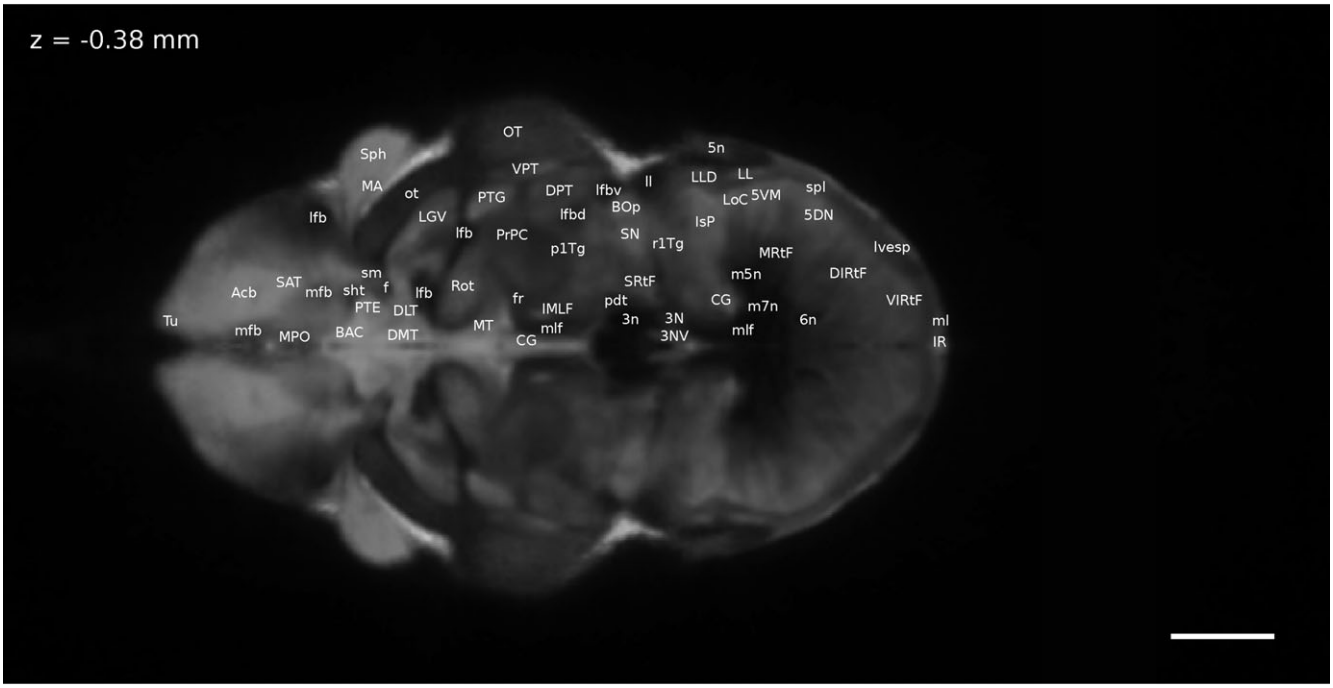

FIGURE 25

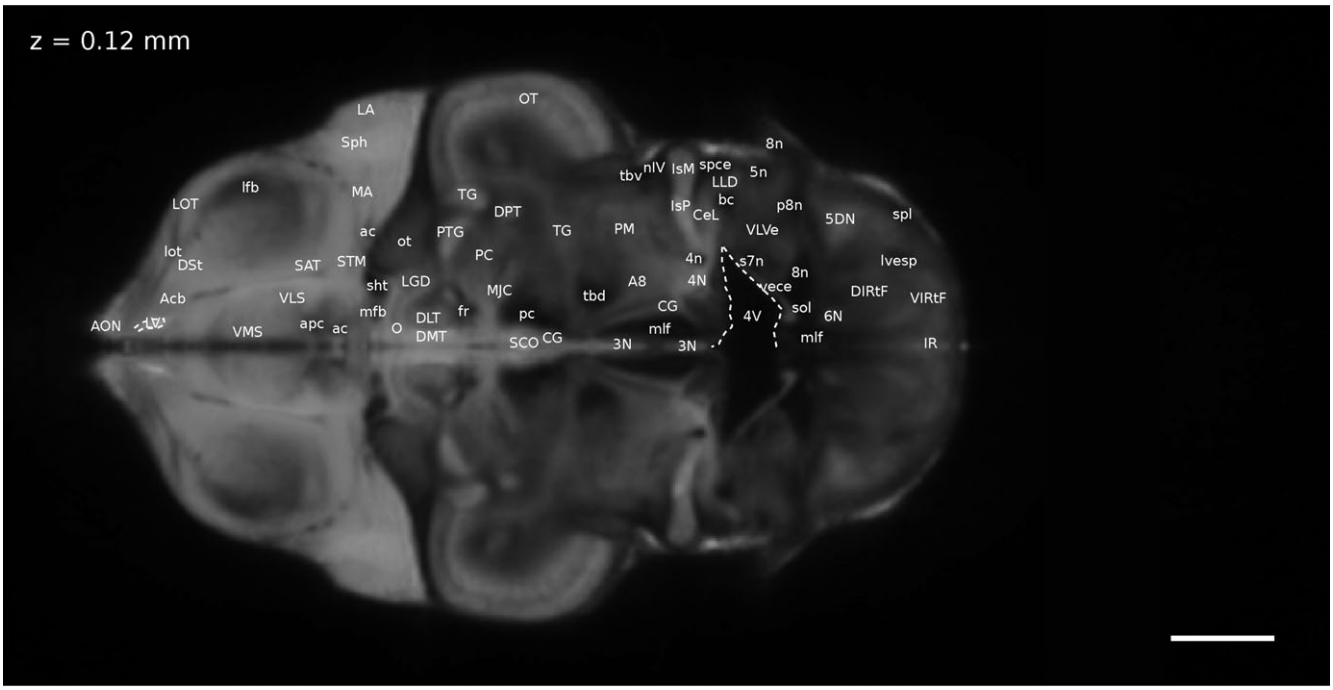

FIGURE 26

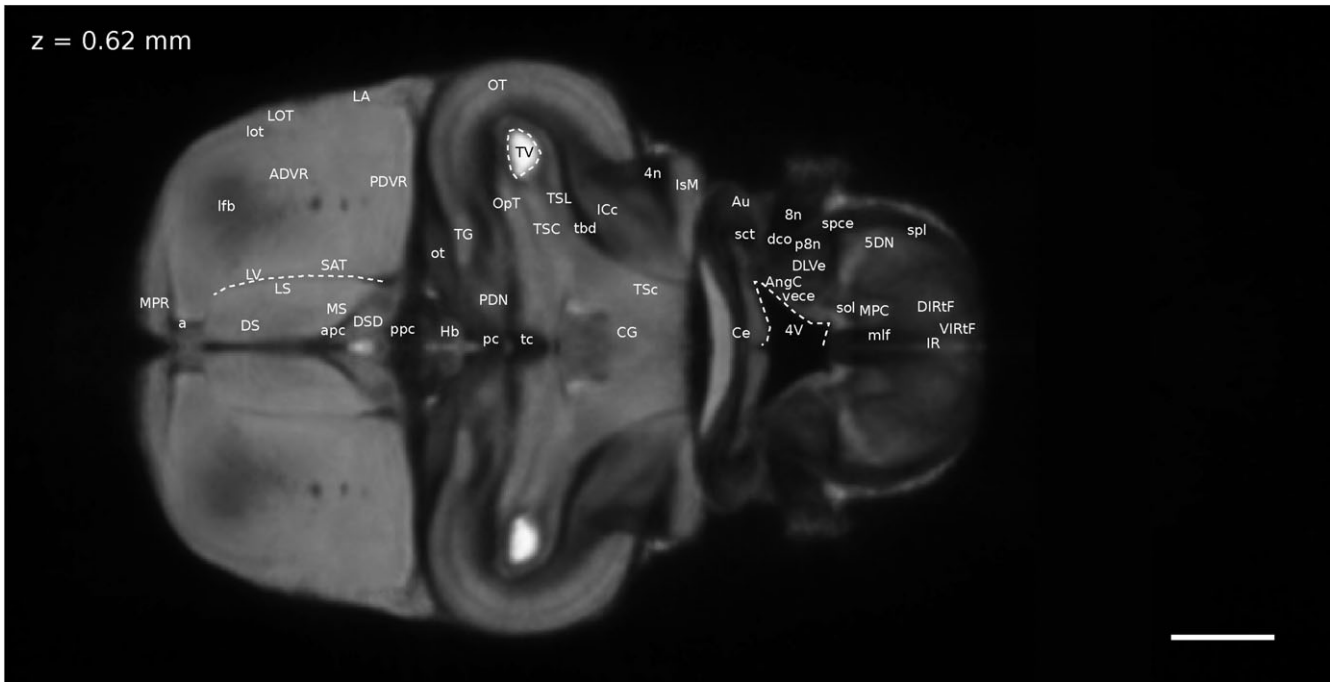

FIGURE 27

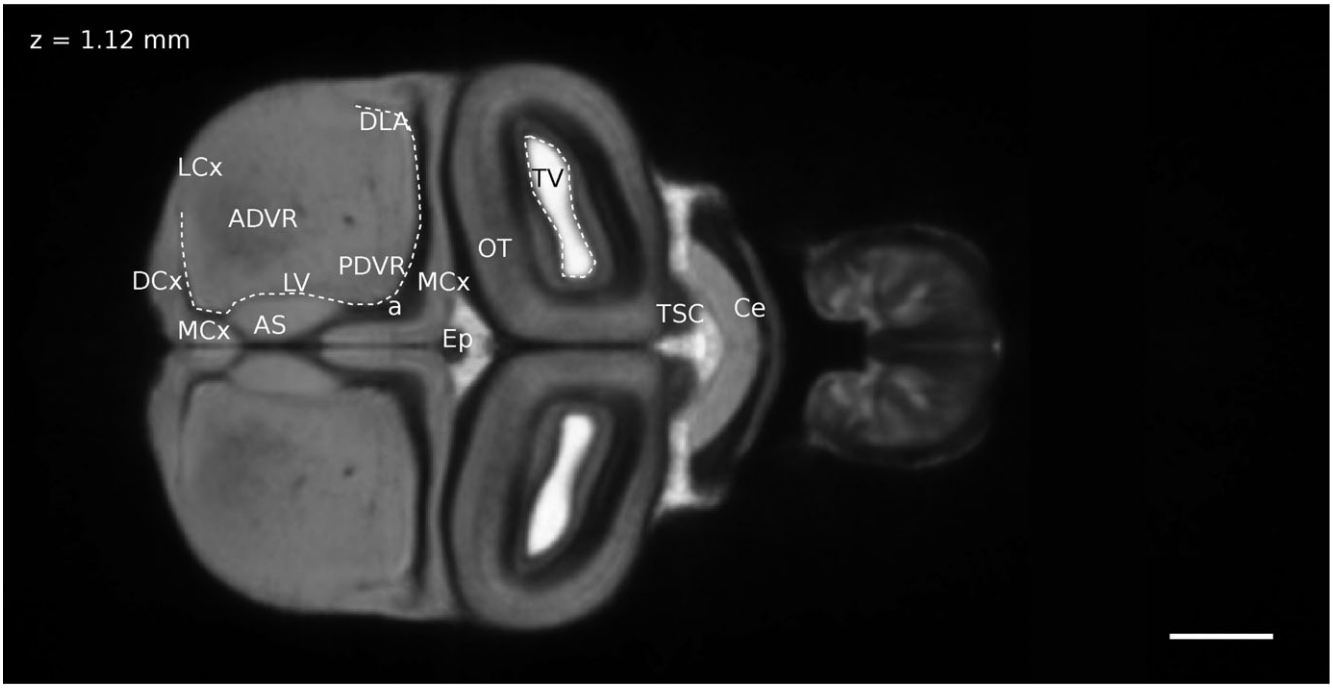

FIGURE 28

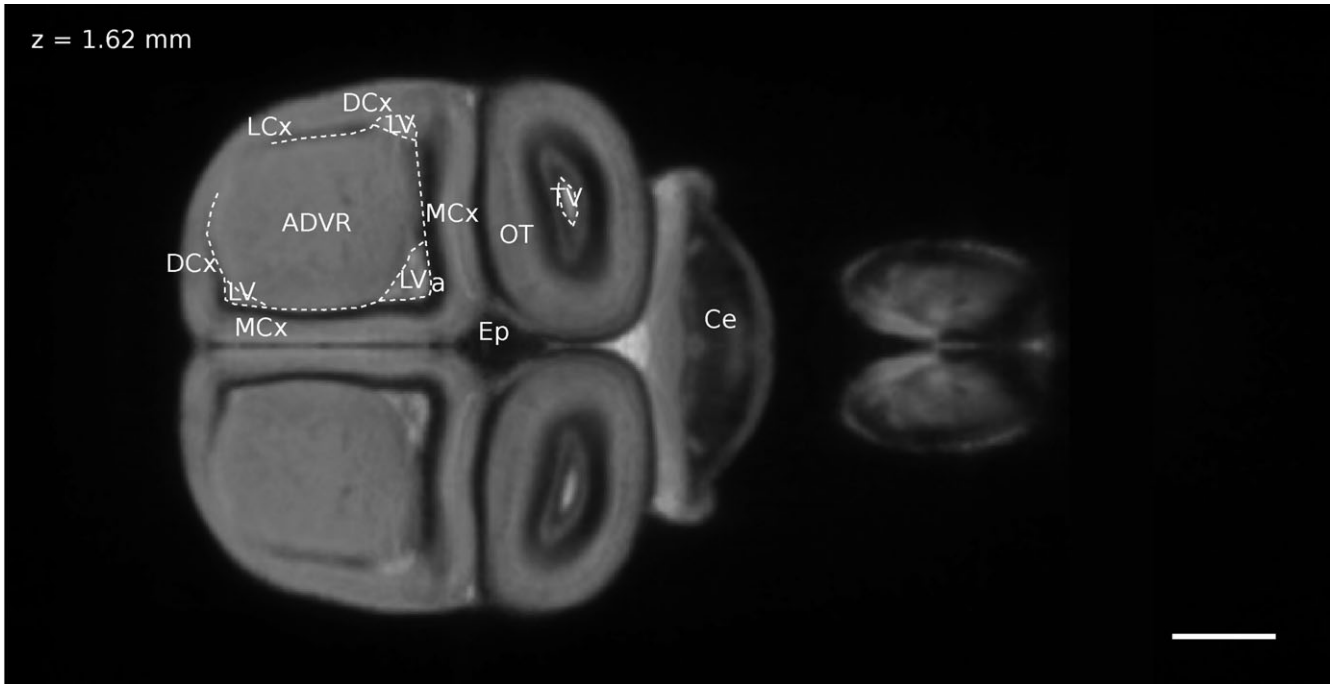

FIGURE 29

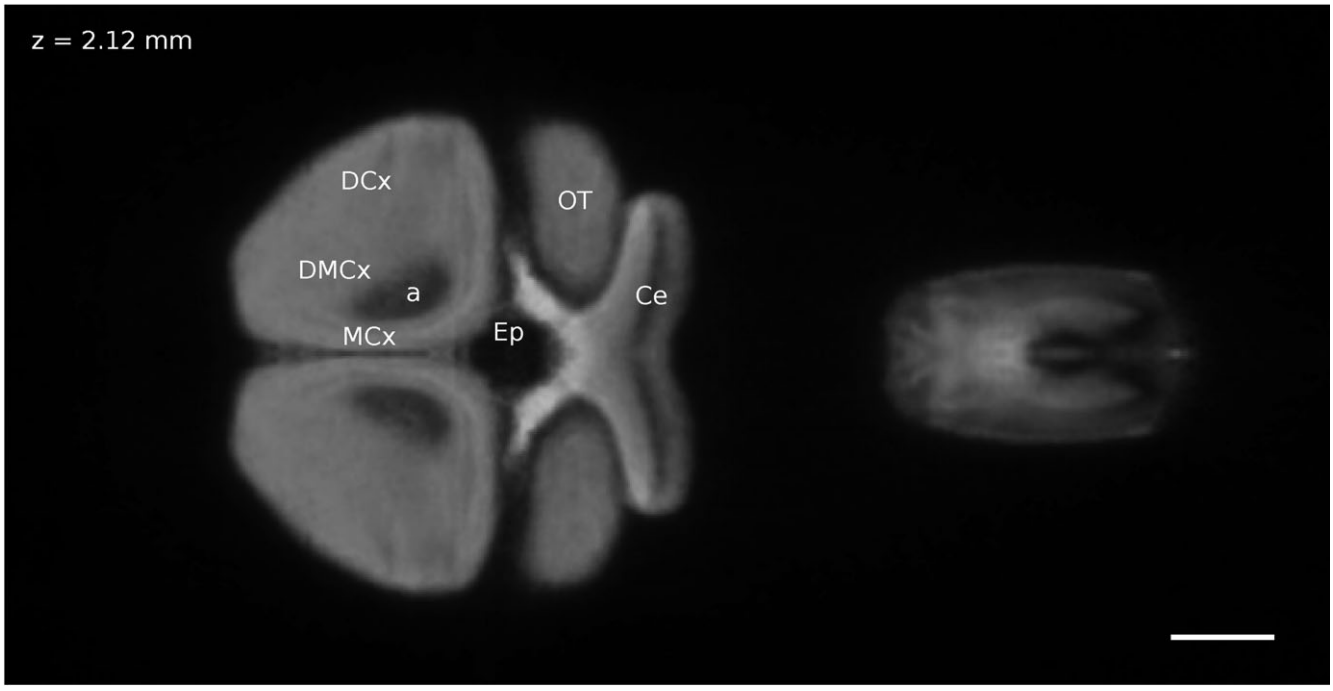

FIGURE 30

FIGURES 31–36 Sagittal sections through the MRI model of the tawny dragon (*Ctenophorus decresii*) brain. Figures are in medio-lateral order. Each section is 25 voxels or 500 μm lateral to the previous section except for Figure 32, which is 20 voxels (400 μm) lateral to Figure . This is because Figure is offset from the midline by 100 μm. The plane of each section according to our coordinate system is indicated in the upper left corner. The bar in the lower right corner = 1 mm. A list of abbreviations is found in Table 1

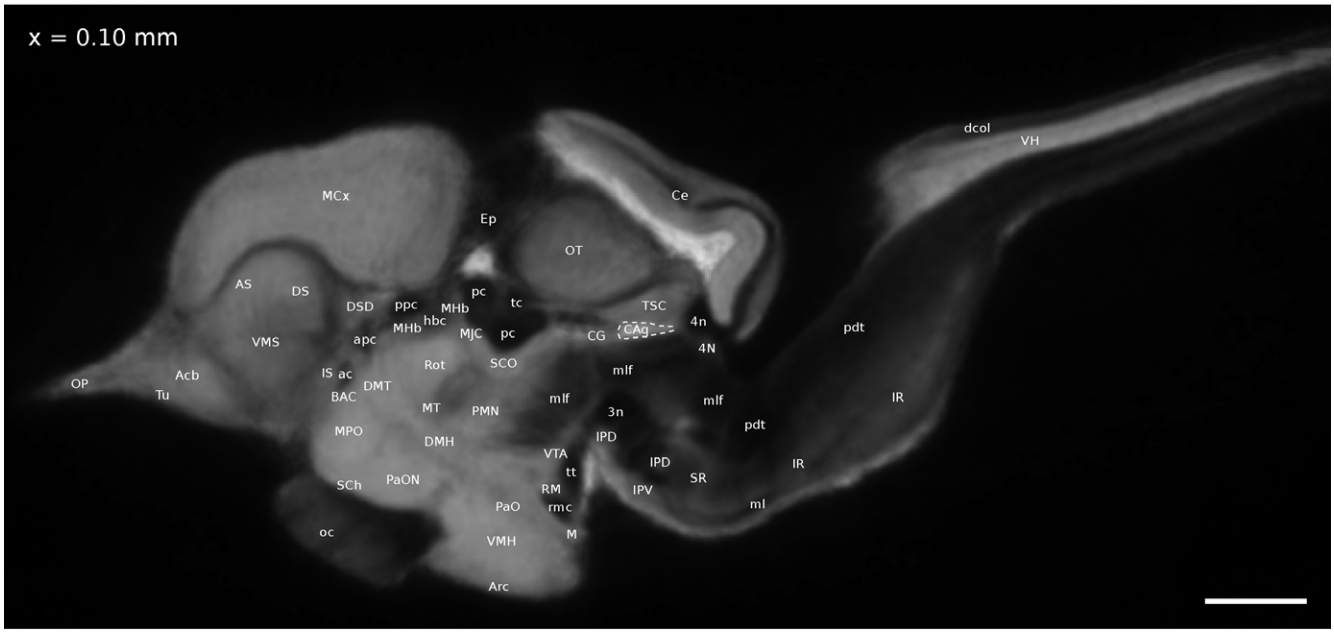

FIGURE 31

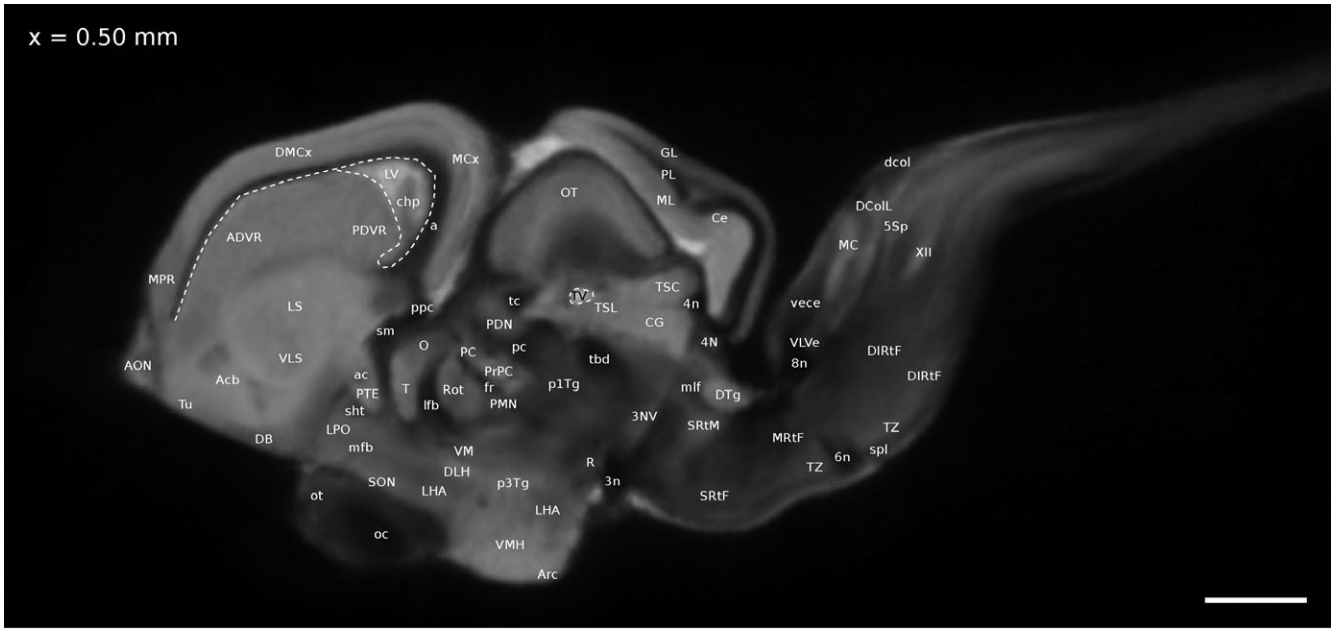

FIGURE 32

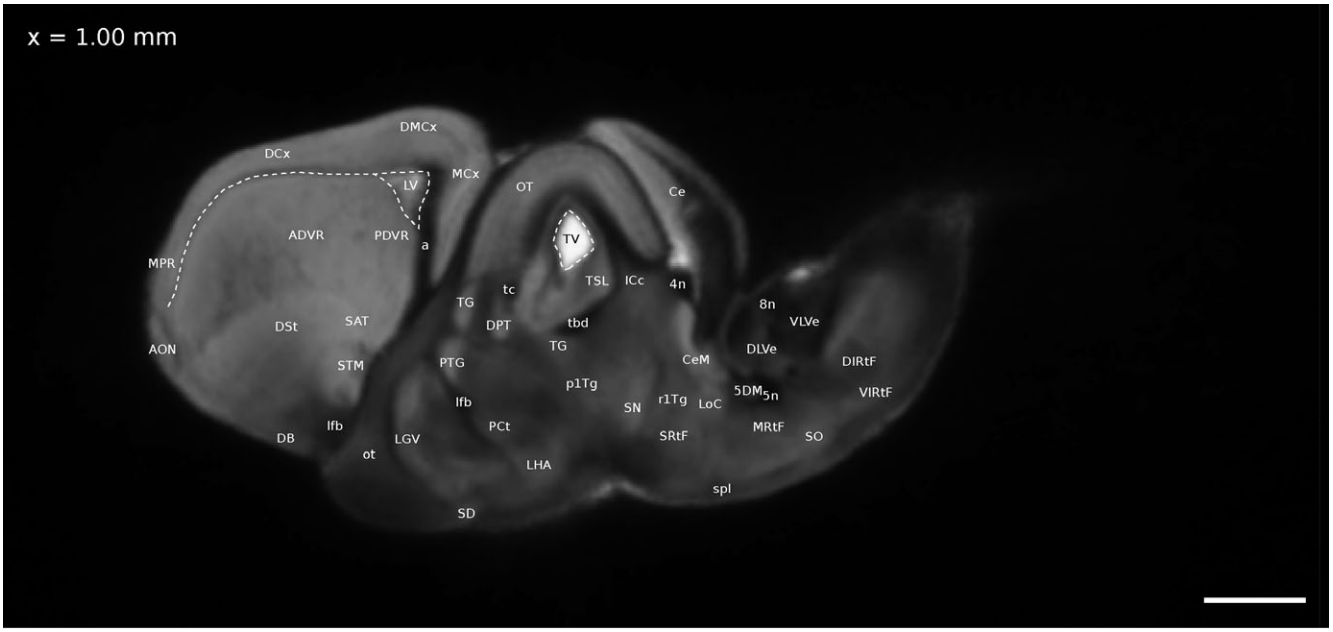

FIGURE 33

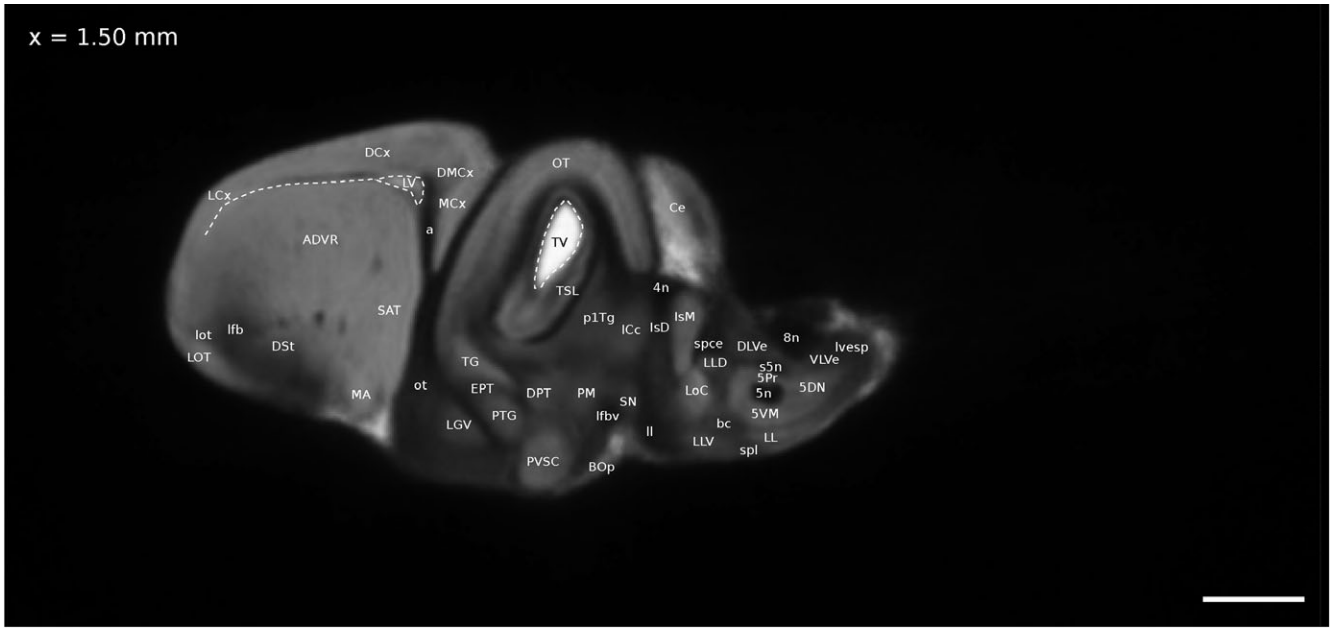

FIGURE 34

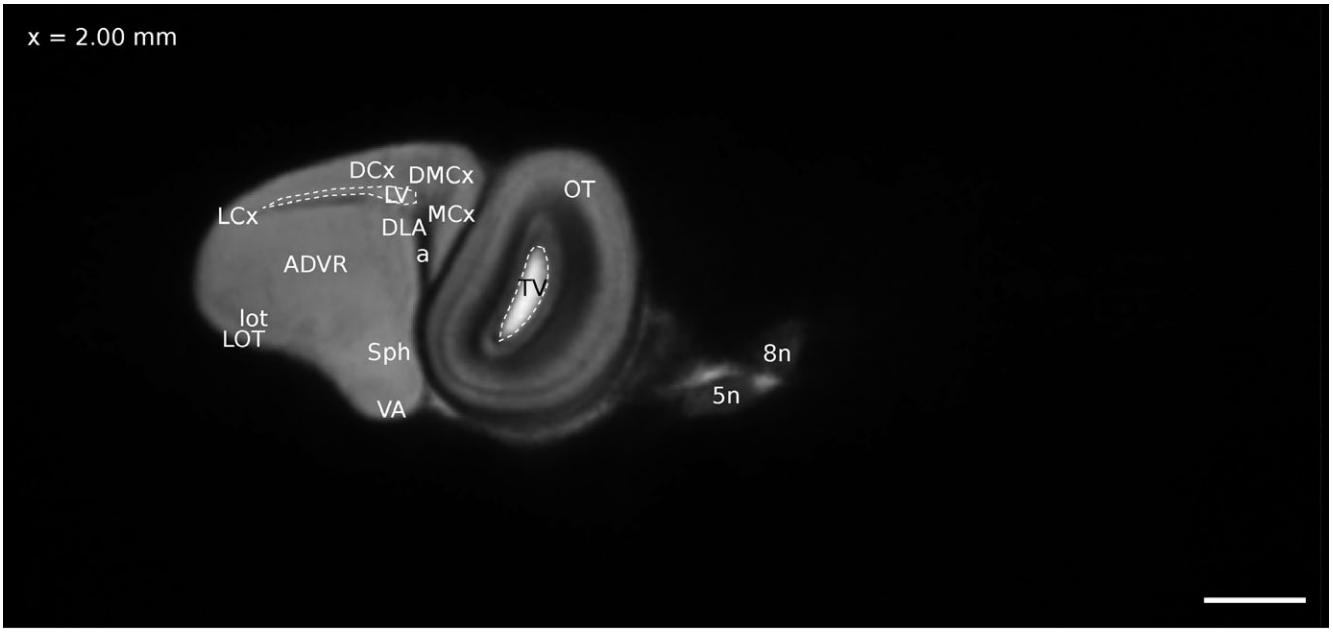

FIGURE 35

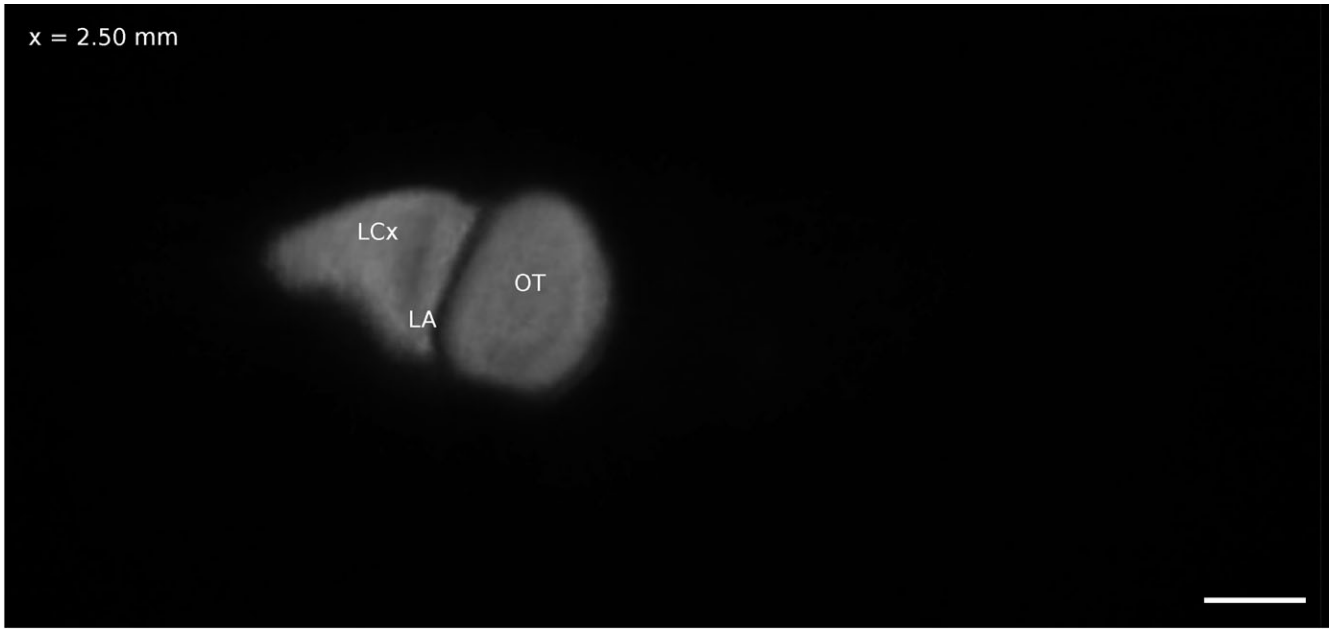

FIGURE 36